chemosensors

MDPI

Review

Materials for Chemical Sensing: A Comprehensive Review on the Recent Advances and Outlook Using Ionic Liquids, Metal–Organic Frameworks (MOFs), and MOF-Based Composites

Valentina Gargiulo [1], Michela Alfè [1,*], Laura Giordano [2] and Stefano Lettieri [3,*]

[1] Institute of Sciences and Technologies for Sustainable Energy and Mobility, National Research Council (CNR-STEMS), P.le V. Tecchio 80, 80125 Napoli, Italy; valentina.gargiulo@stems.cnr.it
[2] Institute of Marine Sciences, National Research Council (ISMAR-CNR), Calata Porta di Massa, 80133 Naples, Italy; laura.giordano@cnr.it
[3] Institute of Applied Sciences and Intelligent Systems "E. Caianiello", National Research Council (CNR-ISASI), Complesso Universitario di Monte S. Angelo, Via Cupa Cintia 21, 80126 Napoli, Italy
* Correspondence: michela.alfe@stems.cnr.it (M.A.); stefano.lettieri@isasi.cnr.it (S.L.)

Abstract: The ability to measure and monitor the concentration of specific chemical and/or gaseous species (i.e., "analytes") is the main requirement in many fields, including industrial processes, medical applications, and workplace safety management. As a consequence, several kinds of sensors have been developed in the modern era according to some practical guidelines that regard the characteristics of the active (sensing) materials on which the sensor devices are based. These characteristics include the cost-effectiveness of the materials' manufacturing, the sensitivity to analytes, the material stability, and the possibility of exploiting them for low-cost and portable devices. Consequently, many gas sensors employ well-defined transduction methods, the most popular being the oxidation (or reduction) of the analyte in an electrochemical reactor, optical techniques, and chemiresistive responses to gas adsorption. In recent years, many of the efforts devoted to improving these methods have been directed towards the use of certain classes of specific materials. In particular, ionic liquids have been employed as electrolytes of exceptional properties for the preparation of amperometric gas sensors, while metal–organic frameworks (MOFs) are used as highly porous and reactive materials which can be employed, in pure form or as a component of MOF-based functional composites, as active materials of chemiresistive or optical sensors. Here, we report on the most recent developments relative to the use of these classes of materials in chemical sensing. We discuss the main features of these materials and the reasons why they are considered interesting in the field of chemical sensors. Subsequently, we review some of the technological and scientific results published in the span of the last six years that we consider among the most interesting and useful ones for expanding the awareness on future trends in chemical sensing. Finally, we discuss the prospects for the use of these materials and the factors involved in their possible use for new generations of sensor devices.

Keywords: gas sensors; ionic liquids; metal–organic frameworks; MOF-based composites; optical sensors; chemiresistors; electrochemical sensors; oxygen; hydrogen; chemical sensing

Citation: Gargiulo, V.; Alfè, M.; Giordano, L.; Lettieri, S. Materials for Chemical Sensing: A Comprehensive Review on the Recent Advances and Outlook Using Ionic Liquids, Metal–Organic Frameworks (MOFs), and MOF-Based Composites. *Chemosensors* **2022**, *10*, 290. https://doi.org/10.3390/chemosensors10080290

Academic Editors: Andrea Gaiardo, Barbara Fabbri and Vincenzo Guidi

Received: 11 June 2022
Accepted: 19 July 2022
Published: 22 July 2022

1. Introduction

It is widely recognized that the development of technologies suitable for the identification and measurement of concentration of gaseous species is of great significance in many fields, including, for example, public health and safety, energy, climate, and environmental risk assessment. While it is clear that useful sensing devices (also referred to as "sensors") must fulfill analytical standards, it is important to underline that other additional requirements exist, whose relative importance may vary depending on the specific application. Here, we can mention, for example: low production and consumption costs, small sizes,

device portability for in-field measurements, possibility to transmit the data remotely, and so forth. A couple of examples of public documents available on the web are given here [1,2] as references for the economic figures involved.

The need to monitor the concentration of several kinds of gases ("analytes") is recurring or, more appropriately, constantly present in many industrial processes, medical activities and everyday life activities. Due to this, several kinds of gas-sensing devices—based on different technologies and on different gas-sensitive materials—have been developed in the modern era [3–9]. Hence, a review on gas sensors and on the related technologies can be organized in different ways, such as by focusing on the transduction technology, on the specific application in which given sensors are employed, on the analyte to be revealed or, finally, on the active materials which allow sensing the gas molecules.

The present review is organized according to the latter criterion and is structured in sections dedicated to different typologies of materials. In particular, we review here some more recent developments in the use of ionic liquids and metal–organic frameworks (MOFs) in chemical sensing. Regarding the latter class of materials, the present review considers both MOFs used in pure form and, more extensively, composite materials in which a MOF is a component of the active sensing materials. In more detail, we will discuss hybrid materials in which MOFs are integrated with metal oxides, carbon-based materials, metal nanoparticles, and conducting polymers.

For the sake of clarity, we will first spend the first part of this introduction by pointing out (i) some of the applications requiring the use of chemical sensors and gas sensors, (ii) some of the most important analytes which are extensively considered in the present review, and (iii) the physical/chemical mechanisms for the detection and concentration measurements of the gaseous species which are at the basis of the kind of sensors considered in this work.

Among the most important fields that involve or require gas sensing and concentration measurements, we shall mention at least: (i) environmental monitoring, which includes, for example, the control of indoor air quality [6,10,11] and the analysis of air pollution caused by vehicular traffic [12,13]; (ii) human safety, including the detection of harmful and/or explosive gases [14–17]; and (iii) medical application and diagnoses, such as breath and blood analysis [18,19]. A large variety of applications exist in reference to these fields, whose review is below the scope of the present work. It is worth mentioning that almost any (if not, any) monitoring activity has to be performed on-site and that measurements shall be collected in real time for various reasons (consider, for example, the case in which sensors have to monitor an industrial process or the leakage of some toxic species in an enclosed area). Moreover, prolonged monitoring is very often also needed, so the cost-effectiveness of running the sensor device is also an issue. This variety of applications and requirements explains why a wide array of sensing devices have been developed in recent decades [3–26].

The development of gas-sensing devices is in many cases focused on the detection of toxic or harmful gases generated by industrial processes or automobiles, such as NO and NO_2 (NO_x), CO, CO_2, SO_2, O_3, and NH_3. Other species to be mentioned are volatile organic compounds (VOCs), namely, organic compounds of small molecular mass which vaporize easily at room temperature such as acetone (CH_3CH_3CO), formaldehyde (HCHO), ethanol (CH_3CH_2OH), benzene (C_6H_6), toluene (C_7H_8), and others [16].

Molecular oxygen (O_2) is another analyte of importance. The possibility to detect it and to measure its partial pressure in air or, in most cases, when dissolved in some liquid medium (e.g., water or blood) is of paramount importance for many applications, such as medicine (e.g., the measurement of O_2 concentration in blood or in breath for medical diagnoses), plant biology, marine and freshwater research, and food technology and packaging. Several examples on the applications of O_2 sensing and extended references on the methods to achieve it are reported in excellent reviews [27–29].

The different physical/chemical mechanisms for the detection and concentration measurements of the gaseous species correspond, of course, to different classes/families of materials. However, gas-sensing materials shall ideally share some key characteristics,

regardless of the transduction mechanism, the main and most obvious one being a large specific surface area (SSA). An exhaustive (although incomplete) list of possible approaches to gas sensing can be summarized as in Table 1.

Table 1. Types of sensor devices and their principle of operation.

Sensor Type	Examples	Principle of Operation
Electrochemical	Amperometric, ChemFET	Analyte molecules are involved in the redox reaction at the working electrode of an electrochemical cell, modulating the electrical current.
Electrical	Chemoresistors	Adsorbed molecules of the target gas interact with oxygen species adsorbed on the surface of a nanoparticulated semiconductor, modifying its charge depletion regions and its electrical conductivity.
Gravimetric	Surface acoustic waves, piezoelectric	A vibration resonance frequency is modified due to the adsorption of the target analyte. The shift in resonance frequency quantifies the analyte concentration.
Thermochemical	Catalytic bead sensors	The target gas is burnt, causing a temperature rise that changes the resistance of the detecting element of the sensor proportional to the concentration of combusted gas.
Optical	Absorptive Reflective Fluorescence-based	Adsorbed molecules of the target gas modify in several ways the optical properties of the sensing material (e.g., reflectivity, optical transmission, fluorescence spectrum and/or lifetime, etc.).

As the gas sensors represented in Table 1 operate on different principles, the physical and chemical characteristics of the materials on which they are based are also different. In this work, we mainly deal with functional and composite materials operating via electrochemical, electrical, or optical mechanisms, so we will briefly discuss only them.

As mentioned, we will review recent developments in the use of ionic liquids (ILs) and metal–organic frameworks (MOFs) in gas sensing. Section 2 gives a brief discussion on the basic mechanisms for gas sensing which are employed in the sensing devices by use of the materials reviewed here, while Sections 3 and 4 review some recent literature results (mostly from 2016 to 2021) on the use of the mentioned class of materials for gas sensing. The main role of ILs is played in the context of sensor devices based on electrochemical cells, also known as amperometric gas sensors. Regarding MOFs, a major part of the references reviewed here deal with their use in MOF-based chemiresistive composites, although the versatility of MOFs allows their use also as stand-alone sensing materials based on other kind of responses (e.g., luminescence response, chemicapacitive response, mechanical response, magnetic response, and others).

2. Sensing Methods: Amperometric Sensors, Fluorescence-Based Sensors, and Chemiresistors

As the goal of the present work is to review recent developments of some specific classes of materials and systems, we will only consider a few of the possible approaches/methods for gas sensing reported in Table 1. Ionic liquids are mostly used in the context of electrochemical gas sensors, in particular to provide specific and advantageous characteristics to the electrolyte medium. MOFs are involved mostly as fluorescence-based (optical) gas sensors, while a substantial number of examples exist in which they are involved as sensing elements in chemiresistors. These are thus the methods summarized here.

2.1. Amperometric Electrochemical Gas Sensors

As indicated by the name itself, an amperometric gas sensor (AGS) operates by correlating a local concentration of gas with the amplitude of an electric current. This kind of transduction scheme (i.e., gas concentration to electrical current) has several advantages and is quite popular due to its low cost, good sensitivity, possibility to miniaturize the devices, and low power consumptions.

The precise mechanism over which an AGS operates is based on a redox reaction of the gas analyte once it is adsorbed on a suitably polarized working electrode that operates in an electrochemical cell. The reaction can be an oxidation or a reduction, which, respectively, confer an electron or a hole to the working electrode, causing an electrical current to run into the electrochemical circuit. The amplitude of such a current is proportional to the concentration of the gas analyte.

The first amperometric gas sensors were reported by Leyland Clark et al. [30,31] for the purpose of measuring the oxygen partial pressure in blood. The schematic design of a Clark-type gas sensor is reported in Figure 1, showing the main components of the device, i.e., a membrane that keeps the undesired chemicals separated from the electrochemical cell and allows the diffusion of the gas analyte, an electrolyte that solvates the gas molecules and diffuses them toward electrodes. The solvated molecules that diffuse toward an appropriately polarized electrode ("working electrode" in Figure 1) where they are subjected to an electrochemical oxidation or reduction ("redox", in short) reaction. The role of the counter electrode (CE) is to counter the half-reaction guaranteeing the conservation of charge and allowing the current flow, while the reference electrode allows setting a precise reference for the voltages of the WE and the CE.

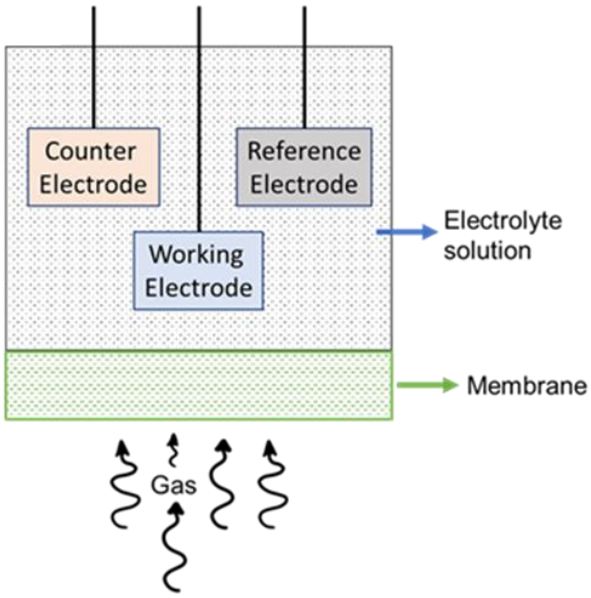

Figure 1. Basic design of a three-electrode Clark-type amperometric gas sensor. The gas flowing from the environment toward the electrochemical cell is filtered by a membrane. As the analyte molecules enter the electrochemical cell, they are solvated by the electrolyte and diffuse into the medium. The solvated molecules that are adsorbed on the working electrode and that pass an additional liquid-phase barrier react with a suitably polarized working electrode and react with it via oxidation or reduction. The counter reaction occurs at the counter electrode, allowing the charge conservation and the flow of current. A third electrode is usually employed as a potential reference.

The current density provided by the redox reaction is proportional to the analyte concentration according to the following equality:

$$I = \left(D_{eff}/L_{eff}\right) nFA \cdot C \quad (1)$$

where D_{eff} and L_{eff} indicate, respectively, the effective diffusion coefficient and the diffusion path of the analyte molecules from the surrounding sensor to the surface of the working electrode, A is the SSA of the electrode, F is the Faraday constant, n is the number of electrons exchanged by the gas molecule in the redox reaction and, finally, C is the concentration of the analyte, i.e., the quantity that has to be determined. Therefore, the

equation indicates that the sensitivity of the apparatus mainly depends on two factors: the SSA of the electrode and the effective diffusion length of the gas molecule in the cell.

The AGSs based on the scheme in Figure 1 are very popular in many applications and, as a matter of fact, there are commercially available devices based on them [9,32]. Nevertheless, Clark-type sensors based on the simplest design have some peculiar drawbacks. The main issue is related to the limit of detection of the devices, which is discussed later. Another one is the fact that the average lifetimes of such devices are limited by the evaporation of the solvent, making their use in very dry and/or hot environments unsuitable. This last issue is one of the main reasons why the use of ionic liquids as electrolytes was introduced.

As mentioned, the sensitivity of standard Clark-type sensors using noble metals (e.g., Pt) as electrodes is an issue for applications that require low values for the limit of detection (LOD). While the first devices were adequate for the measurement of blood oxygenation, the device sensitivities associated with the use of standard electrodes are usually not sufficient to measure gas concentrations of the order of a few parts per million (ppm) which are required to detect alarming concentrations of toxic/polluting gases.

LODs in the range of alarm levels for toxic gases are achieved without special effort with chemiresistive sensors, as a consequence of the nanostructured and microporous morphology of thick, polycrystalline, metal oxide films used in these devices. Therefore, it can be deduced that an increase in the LOD of AGS has to be pursued by increasing the surface area of the working electrode. Such an increase is difficult to achieve by using simple noble-metal electrodes, due to their intrinsic cost.

Hence, the practical way to improve the performance of AGS is to modify the electrode morphology. To this aim, new approaches have been developed. An important one consisted of substituting the porous membrane shown in Figure 1 with a porous gas diffusion electrode (GDE), consisting of polymer membranes made of a porous polymer (usually PTFE), which embed fine grains of some metal [33]. This modification is technically very significant, as it allows both decreasing the diffusion path of the gas analyte and enhancing the surface area of the working electrode. Another improvement in the performance of AGS devices is in their use as membranes of solid polymer electrolytes (SPEs), i.e., membranes made of polymers (e.g., Nafion) that allow ionic conduction. Such SPEs act not only as membranes but also as solid electrolytes.

The idea of using ionic liquids (ILs) as the electrolyte for an AGS is the topic of the next section: it was firstly proposed and investigated in 2004 [34] and is currently adopted in many devices [35]. In this work, we will focus on recent developments in this field, mostly covering works in the years from 2016 to 2021.

2.2. Chemiresistive Gas Sensors

Chemiresistors transduce the chemical signal (i.e., gas concentration) into an electrical signal (i.e., conductivity). This is obtained via the chemiresistive effect, which requires a semiconductor material as the gas-sensitive element. Gas molecules adsorbed on the semiconductor surface modulate (via several mechanisms) the spatial width of charge-depleted regions, affecting the electrical conductivity of the material. While the effect can be negligible for bulky single crystals, it becomes much more relevant when occurring in isolated nanostructures (e.g., nanorods) or in nanoparticle films because in these cases, any enlargement of the depletion region hinders very effectively the transport of charge carriers. This underlines the importance of preparing semiconductor materials with a large specific surface area.

The materials mostly employed in electrical gas sensors belong to the class of metal oxides, thanks to their large chemiresistive effect [3,4] and to the availability of many physical [36–41] and chemical [42–44] preparation methods that allow obtaining thick-film sensors with large specific surface areas. However, the use of chemiresistors is by no means limited to metal oxides. Other functional materials have been employed as the active (gas-sensing) element of chemiresistors, among which carbon nanotubes [45] and graphene [46] deserve a special mention, along with, particularly in recent years, 2D materials [47] and

MOFs [48,49]. For the sake of this review, chemiresistors using this last class of materials as a key component of the sensing element are considered.

2.3. Optochemical and Photoluminescence-Based Sensors

Fluorescence-based gas sensors belong to the class of optochemical sensors, a term that indicates devices able to determine the concentration of given analytes by changes in some of the optical parameters of the sensing elements. Hence, this class of devices is based on phenomena that characterize the radiation–matter interaction and/or the light propagation. Examples of such phenomena and of corresponding devices include: optical absorbance and reflection (e.g., devices based on laser spectroscopy), optical refraction (e.g., devices based on optical fibers), light-induced temperature changes (e.g., photothermal detection), light-induced mechanical vibration (e.g., photoacoustic detection), surface waves (e.g., devices based on shifts in surface plasmon resonances), or photoluminescence. The latter case is among the most employed ones and is dominant among the optochemical methods in which metal–organic frameworks are used for gas sensing.

Optochemical sensing exhibits peculiarities and, possibly, advantages over conventional electricity-based sensors. Some advantages of optical gas sensors include: the compatibility and possibility of integration in optical circuits and/or devices based on optical fibers; the low sensitivity to electromagnetic noise; and the possibility to employ more than one physical parameter. This latter point deserves special attention: devices such as chemiresistors are based on changes in a single physical quantity (i.e., the electrical conductivity), while optochemical gas sensors can bring into play and involve various parameters, such as wavelength, polarization, phase, and intensity. Hence, optochemical sensors are inherently multiparameter devices [50]; this circumstance can favor or improve the selectivity of the gas sensors [28,51–53], which is often a major drawback of chemiresistors.

For the sake of this review, we will only consider photoluminescence-based gas sensing, which is based on the changes in photoluminescence (PL) intensity and/or lifetime caused by the interaction between the analyte and the luminescent material. Such a phenomenology can occur via different mechanisms, most of them classified in the class of "photoluminescence quenching" (PLQ) mechanisms.

In many cases, the PLQ in luminescent organic molecules occurs in terms of "collisional quenching" (also often named "dynamic quenching") and is described by the Stern–Volmer equation:

$$\frac{I}{I_0} = 1 + k_q \tau_0 [Q] \quad (2)$$

where I and I_0 indicate the PL intensity in presence of the "quencher" (see below for the meaning of this term), k_q is a constant dependent on the specific fluorophore-quencher interaction, τ_0 is the PL lifetime in the absence of the quencher, and $[Q]$ is the quencher concentration, i.e., the quantity that has to be determined via PL measurements.

Equation (2) describes the quenching of photoluminescence caused by one (or more) intramolecular deactivation processes, in which a "quencher" molecule Q (which represents the analyte in PLQ-based gas sensors) affects/accelerates the decay rate of the fluorophore in its excited state. Different deactivation processes can be involved, including intersystem crossing, Dexter electron transfer, and Dexter energy transfer. Due to the intrinsic limitations of this work, these mechanisms cannot be discussed here; for a comprehensive review on the subject, we recommend the classical book by Lakowicz on fluorescence spectroscopy [54]. In any event, the details of these mechanisms are not extremely relevant from a practical point of view, as they all lead to a phenomenological law well described by Equation (2), which can be used to calibrate the actual concentration of the quenching analyte via the measurement of PL intensity.

As already mentioned previously, collisional quenching affects the decay rate, so that both the values of PL intensity and the luminescence lifetimes change during the interaction between the fluorophore and the analyte. From a technical point of view, this

is an important point as measurements based on lifetimes are usually more reliable than those based on intensity. Actual commercial devices, in fact, are based on lifetime changes.

The collisional quenching is mostly involved for dioxygen (O_2) optical sensors, which are mainly based on metal–ligand complexes that undergo collisional quenching (via intersystem crossing) interacting with O_2 [27,55–57]. Frequently investigated O_2-sensitive fluorescent molecules (also referred to as O_2 indicators) are coordination complexes containing platinum (Pt) or ruthenium (Ru) atoms, such as platinum(II) octaethyl-porphyrin (PtOEP) [58–60], platinum(II)-5,10,15,20-tetrakis-(2,3,4,5,6-pentafluorphenyl)-porphyrin (PtTFPP) [61–63], and tris(4,7-diphenyl-1,10-phenanthroline)ruthenium(II) dichloride complex (Ru(dpp)) [64,65]. However, it is worth mentioning that also some metal oxides, including ZnO [66–68], TiO_2 [69], MgO [70], and SnO_2 [71,72], have been shown to act in a manner very similar to a collisional quencher, although some targeted investigations [73,74] suggest that the mechanisms active for these cases are slightly different and involve "static" quenching, i.e., a modification of intensity, only not accompanied by changes in the lifetime. This point is still not completely investigated and might be relevant for the future investigation of inorganic photoluminescent indicators. It is also worth noting that the study of gas-induced PL modifications in metal oxides or in metal-oxide-based heterostructures can be relevant in terms of the study of basic charge-carrier-recombination mechanisms. Their precise understanding is crucial when the material also exhibits photocatalytic properties, as in the case of TiO_2 [75,76].

3. Ionic Liquids in Amperometric Gas Sensing—Recent Developments

Ionic liquids (ILs) are among the materials of interest for the development of improved amperometric gas sensors. Among their main characteristics, it is worth emphasizing their versatility, intended in reference to the broad range of the properties that they share [77–79].

Before discussing their applications, it is useful to sketch a general description of ILs. Generally speaking, ionic liquids are salts at the liquid state. However, the commonly used terminology restricts this definition, making a distinction between "room-temperature ILs" (also RTILs) which are liquid at room temperature and proper ILs, which are solid at room temperature but whose melting point is below 100 °C [80] or below some other conventional temperature larger than the room temperature. As evidenced by the name itself, ionic liquids are mostly made by ions, typically a small anion (either organic or inorganic) and a large organic cation. The type and the size of each of the ions determine the properties of a given ionic liquid. It can be generally stated that the cation affects the physical properties of the salt, while the anion affects its reactivity and chemical behavior. Some of these properties are specifically relevant for the case of interest, i.e., the use of ILs in amperometric sensing.

To begin with, we mentioned before that one major drawback of gas sensors based on electrochemical cells is that their usage is limited by the evaporation of the liquid electrolyte. This fact is one of the main drivers towards the use of ILs, as they are extremely nonvolatile. Other advantages of ILs include their intrinsic conductivity, high chemical stability, high viscosity, and wide electrochemical window. It is worth briefly discussing some of these properties.

Electrical conductivity and viscosity: The room temperature electrical conductivity of an ionic liquid is typically in the range of (about) 0.1–20 mS cm^{-1}. These conductivity values are smaller than those of common aqueous electrolyte solutions. This fact can be seen as a consequence of the relationship between the viscosity (η) and electrical conductivity (Λ) of an electrolyte solution, known as empirical Walden's rule, stating that their product is constant at a given temperature, i.e., $\Lambda\eta = const$. As this relation is empirically obeyed by both regular electrolyte solutions and ionic liquids [81], the viscosity is typically much larger in the latter with respect to the former. Typical values for η at room temperature range from 10 to 10^5 cP (centipoise) in ionic liquids, while values ranging from 0.1 to 10 cP are common for standard solvents. Considering the Walden's rule, the mentioned electrical conductivity values lower than those typical for aqueous solutions of standard electrolytes

are explained. This point represents a major obstacle for applications, as the lesser electrical conductivity is accompanied by a lesser diffusion rate and by a decrease in the rate of reaction and separation processes.

Electrochemical window: The electrochemical window of a substance (e.g., a solvent) is, by definition, the electrode electric potential range between which the substance is neither oxidized nor reduced. It is important to determine the value of this quantity for both solvents and electrolytes when solutions are used in electrochemical applications. Large electrochemical windows of liquid solvents are favorable, as they allow the development of reactions involving solute molecules instead of unwanted reactions of the solvent. In the case of aqueous solution, the electrochemical window is about 1.23 eV, outside of which the electrolysis of water occurs. This value is regarded as relatively small. Conversely, the electrochemical window of ionic liquids is much larger, ranging from 4 to 5 volts typically, although higher values have been reported [82]. It is worth mentioning that the electrochemical window is sensibly affected by impurities in the ionic liquid, which have to be kept in control to avoid affecting the stability of the electrochemical cell.

The following Table 2 reports some references on AGS using ILs as solvents, starting from the year 2016 and ordered by analyte.

Table 2. References on AGS using ionic liquids (ILs) as solvents, ordered by analyte.

Analyte	Ionic Liquid	Electrode	Analyte Concentration	Ref.
O_2				
	[C4mpyrr][NTf2]	Clark-type sensor with polycrystalline Pt gauze	1–20%	[83]
	[C2mim][NTf2] and [C4mpyrr][NTf2]	Screen-printed (SP) electrodes	10–100% and 0.1–5%	[84]
	[N8,2,2,2][NTf2]	Pt MATFE	10–100%	[85]
	[C2mim][NTf2]	Pt microdisk and Pt MATFE	0.1–100%	[86]
	[MOmim][PF6]	Au microchannel electrode	5000–25,000 ppm	[87]
	[Bmim][BF4]	Au interdigitated electrodes	20–100%	[88]
	[C4mpyrr][NTf2]	Au on porous PTFE substrate	5–20%	[89]
	[C2mim][NTf2] and [C4mim][PF6]	SP electrodes (graphite)	0.1–20% and 100%	[90]
	[C4mpyrr][NTf2]	Au microchannel electrode	50–400 ppm and 2000–5000 ppm	[91]
	[C4mpyrr][NTf2]	Clark-type sensor with polycrystalline Pt gauze	5–20%	[92]
	[C4mpyrr][NTf2]	Interdigitated electrodes	1400–4800 ppm	[93]
	[C4mim][PF6], [C2mim][PF6] and [C5mim][PF6]	Pt interdigitated electrodes	0–100%	[94]
	[C4mim][BF4]	Planar electrodes	20–100%	[95]
	[Bmim][BF6]	Pt planar electrodes modified by NiCo2O4/rGO/[Bmim][BF6] composite	20–100%	[96]
	[C4mpn][Br]	Pt microelectrodes, 1% Ag-coated chitosan added to the IL	20–100%	[97]
	[Bmim][BF4]	SPE, solid polymer electrolyte (PTFE/Carbon nanotubes/IL)	2.1–12.6%	[98]
	[Emmim][TFSI] and [Bmim][TFSI]	Pt electrodes, IL + reduced graphene (rGO) + α-Fe_2O_3 electrolyte	20–100%	[99]
	[C2mim][NTf2]	IL membrane on Au-TFE	20–100%	[100]
	[C2mim][NTf2] added with Poly[DADMA][NTf2]	IL/poly(IL) membrane on Au-TFE	20–100%	[100]
O_2 and **NH_3**	[C2mim][BF4] and [C4mim][BF4]	Gel polymer electrolyte (ILs in PVDF) between planar electrodes	1–20% for O_2; 1–10 ppm for NH_3	[101]
O_2 and **H_2**	[Bmpy][NTf2]	Planar Pt-Ni alloy electrodes	500–5000 ppm for O_2; 500–6250 ppm for H_2	[102]

Table 2. *Cont.*

Analyte	Ionic Liquid	Electrode	Analyte Concentration	Ref.
H_2	[C4mim][NTf2] and [C4mpyrr][NTf2]	Clark-type sensor with polycrystalline Pt gauze	0.05–1.25%	[103]
	[C4mim]Cl	Pd deposited on carbon gas diffusion electrode	1–5%	[104]
	[Bmpy][NTf2]	[Bmpy][NTf2] on Pt/C/Nafion screen-printed electrode	2000–10,000 ppm	[105]
	[C2mim][NTf2]	Au microchannel electrodes with electrodeposited Pt nanoparticles	0.1–10%	[106]
NH_3	[C2mim][NTf2]	Pt SPE, TFE, MATFE, and microdisk	10–100 ppm	[107]
	[C2mim][NTf2]	SP electrode, thin-film electrode (TFE), microarray thin-film electrode (MATFE), and microdisk.	10–100 ppm	[108]
	[C2mim][NTf2]	Pt MATFE	10–100 ppm	[109]
	[C2mim][NTf2]	Pt-based MATFE (with different morphologies)	1–2 ppm LODs (depending on the morphology)	[109]
NH_3 and **HCl**	[C2mim][NTf2] and [C4mpyrr][NTf2]	Au microchannel electrodes	20–100 ppm	[110]
VOC (in air)	[C4mpyrr][NTf2]	Clark-type sensor with polycrystalline Pt gauze	200–3000 ppm of acetaldehyde	[111]
CO_2	[Bmpy][NTf2]	Au microchannel electrodes with electrodeposited Cu nanoparticles	0.14–11%	[112]
Hexanaldehyde (HA)	[Bmim][OH]	Pt microelectrodes	2–300 ppm (HA in squalene)	[113]
C_6H_6 and **HCHO**	[C2mim][$EtSO_4$]	IL and ionogel (IL in poly(N-isopropylacrylamide)) between interdigitated electrodes	10–50 ppm	[114]
SO_2	[C4mpyrr][NTf2]	TFEs and MATFEs	1–10 ppm	[115]
H_2O (humidity)	[Bmim][DCA]	IL incorporated in gels on interdigitated electrodes	30–70% RH	[116]
Ethanol	[Bmim][HSO4]	IL on Au screen-printed electrode	1–10%	[117]
NO_2	[Bmim][NTf2]	Solid polymer electrolyte (PVDF + IL) on screen-printed electrodes	1–10 ppm	[118]
	[Bmim][BF4]	Solid polymer electrolyte (ionic liquid (IL), carbon nanotubes + polyaniline + IL) on SP electrodes	0–700 ppm	[119]
Ethylene (C_2H_4)	[Bmim][NTf2]	Solid polymer electrolyte (PVDF + IL) on SP electrodes	100–500 ppm	[120]

Ionic liquids reported in table: [C2mim][PF6]: 1-ethyl-3-methylimidazolium hexafluorophosphate; [C2mim][NTf2]: 1-ethyl-3-methylimidazolium bis(trifluoromethylsulfonyl)imide; [C4mpyrr][NTf2]: 1-butyl-1-methylpyrrolidinium bis(trifluoromethylsulfonyl)imide; [N8,2,2,2][NTf2]: triethyloctylammonium bis(trifluoromethylsulfonyl)imide; [C4mim][Cl]: 1-butyl-3-methylimidazolium chloride; [C4mim][BF4]: 1-butyl-3-methylimidazolium tetrafluoroborate. [C4mim][PF6]: 1-butyl-3-methylimidazolium hexafluorophosphate; [C4mim][NTf2]: 1-butyl-3-methylimidazolium bis(trifluoromethylsulfonyl)imide; [C5mim][PF6]: 1-pentyl-3-methylimidazolium hexafluorophosphate; [MOmim][PF6]: 1-[8-mercaptooctyl]-3-methylimidazolium hexafluorophosphate; [Bmim][BF4]: 1-Butyl-3-methyl-imidazolium-tetrafluoroborate; [Bmim][NTf2]: 1-Butyl-3-methylimidazolium bis(trifluoromethanesulfonyl)imide; [Emmim][TFSI]: 1-Ethyl-3-methylimidazolium bis(trifluoromethylsulfonyl)imide; [Bmim][NTf2]: 1-Butyl-3-methylimidazolium bis(trifluoromethanesulfonyl)imide; Poly[DADMA][NTf2]: poly(diallyldimethylammonium bis(trifluoromethylsulfonyl)imide).

It is easily seen that the most represented analyte in Table 2 is the (dissolved) oxygen O_2, according to what we already mentioned previously. In many cases, the O_2 concentration entering into the detection cell varied over the entire possible range (i.e., from a few % to 100%). Some of the references reported above also give interesting results on lower concentrations and on the achieved values for the limit of detection (LOD). For example, Lee and coworkers [84] explored ranges of 10–100% (volume concentrations) O_2 by cyclic voltammetry, and of 0.1–5% by long-term chronoamperometry in their work centered on demonstrating that significant improvements in the sensor performances can be achieved via the mechanical polishing of Pt screen-printed electrodes. In particular, the authors reported significant improvements in the LODs for O_2 after electrode polishing, with values as low as 0.1% vol O_2 achieved via long-term chronoamperometry using [C_4mpyrr][NTf_2].

Lower O_2 concentrations were examined in a work by Gondosiwanto and coauthors [91], who explored the range of 40–500 ppm by using as electrodes microstrips of [BMP][Ntf2] loaded with magnetic $CoFe_2O_4$—used as nanostirrers for favoring the gas

diffusion—obtaining values between 9 and 11 ppm as the lowest LODs for O_2 (depending on the electrode preparation).

Apart from O_2, investigations are reported for H_2, NO_2, NH_3, and other species. Concerning the last of the three, interesting LOD(NH_3) values between 1 and 2 ppm have been reported by Hussein and coworkers using highly porous 3D-structured ("cauliflower-shaped") Pt electrodes prepared via electrodeposition [109].

Among the possibilities that have been explored in the various works listed in Table 2 in order to improve the sensing performance, a major one regards the design of the working electrode (WE). As mentioned previously, it is possible to employ porous WE as the initial element encountered by the flowing gas molecules. Alternatively, it is possible to employ a device design in which the gas molecules first partition into the liquid phase and next diffuse towards the WE. An evident advantage of the first design is to improve (shorten) the response time of the device, as the diffusion of gas molecules is usually slow in IL layers. Examples of devices employing a porous WE in Clark-type cell are Refs. [83,92,103,111]. Sensing electrodes are usually in the form polycrystalline Pt gauze materials, while in some cases, these have been functionalized with Pd nanoparticles in order to enhance the reactivity toward the analyte (e.g., [83,104]).

Designs in which the gas first diffuses into the liquid have the advantage (with respect to the previous one) of allowing closer positioning of the electrodes. This allows producing small cells using miniaturized, low-cost electrode geometries, such as screen-printed electrodes (SPEs) or interdigitated electrodes. In such cases, the use of ILs provides a definite advantage over that of conventional electrolytes, as the virtually null volatility of an IL allows the use of small volumes (e.g., [84,90,108]). Similarly, thin-film electrodes (TFEs), interdigitated electrodes, and microarray thin-film electrodes (MATFEs) have been explored in various applications, with many of the most recent ones listed in Table 2.

Another new trend in AGS-based research might be opened by the use of the so-called polyionic liquids, also named as poly(IL)s, which are polyelectrolytes combining the peculiar properties of ILs with the physicochemical robustness/stability of polymers. Poly-ILs have been used in other applications (see Ref. [121] for a review on the subject), but only recently have they been explored as electrolytes of AGS devices in a work by Doblinger and coworkers, who demonstrated the possibility of monitoring the oxidation of NH_3 and the reduction of SO_2 and O_2 using ILs/poly(ILs) membranes on an Au-TFE working electrode [100]. The results suggest that the use of poly(ILs) might be one of the future trends in the exploration of electrochemical gas sensors.

Presently, it is quite established that the use of ionic liquids in AGSs has large potentialities, while room for further increases in the sensitivity of the sensors exists, achievable through suitable combinations of the IL ions, the electrode materials/design, and the kind of electrochemical measurements employed; for a further discussion on this topic and sketches of some perspectives, see Ref. [122].

4. Metal–Organic-Framework-Based Composites in Gas Sensing—Recent Developments

4.1. General Properties of Metal–Organic Frameworks

Metal–organic frameworks (MOFs) are solid porous materials which, according to the terminology officially adopted by IUPAC in 2013, are classified as a subclass of coordination networks which are a subclass of coordination polymers [123]. The MOF network (one-dimensional, two-dimensional, or three-dimensional) arises from the strong coordination bonds between metal nodes (metal ions, metal centers, or metal clusters [124]) and the organic linkers. Usually, transition metal ions, especially those of the first row, lanthanides, and some alkaline earth metals are used as metal nodes because of their variable coordination numbers, geometries, and oxidation states [123,125,126]. Organic molecules containing one or more N-donor or O-donor atoms are mostly used as organic linkers, especially carboxylates (either aliphatic or aromatic containing one or more condensed rings), pyridyl (e.g., pyridine, pyrazine and bipyridyl derivatives), cyano compounds, polyamines,

and imidazole derivatives; in addition, oxalic acid, phosphonates, sulfonates, and crown ethers are other possible ligands [123,125].

The main distinctive structural features of MOFs are the high porosity, the large volume of the pores (up to 90% of the crystalline volume or more), the large specific surface area (above 5000 m^2 g^{-1}), and the good thermal stability (250–500 °C) due to the presence of strong bonds (e.g., C–C, C–H, C–O, and M–O) [123,125]. Many of these properties are determined by the mutual interaction between specific metal ions and linkers; as a consequence, MOFs' characteristics can be tuned by judiciously selecting metal nodes and linkers to have the desired pore size, structure, and functionality for specific applications [127]. MOFs' 3D structure displays cavities and inner surfaces, which are occupied by counterions, solvate molecules and/or guest molecules. The guest species can significantly extend the designed applications of MOFs [127].

MOF synthesis is performed mainly in the liquid phase by mixing solutions of the ligand and metal salts under solvothermal/hydrothermal conditions at a high temperature and pressure. Other alternative and consolidated synthetic strategies are based on mechanochemical, electrochemical (for large-scale synthesis), microwave, and sonochemical methods. The most recently proposed methods are: ionothermal synthesis [123,128], the slow evaporation method [123], the diffusion method [123,129], the use of a microfluidic device [128], dry-gel conversion (DGC) [128] and microemulsion [123].

MOFs are versatile materials which are attracting great interest for application in environmental and biomedical areas as catalysts, as absorbers for toxic gases and metal ions, as materials for electrochemical devices, as drug carriers, as bioimaging agents and also therapeutic agents [130,131]. Recently, MOFs have been used also as sacrificial templates for the production of metal oxides or metal oxide–carbon hybrids [132] with promising morphological and textural properties to be exploited in sensing and electrochemical applications [133,134]. MOFs also are emerging as novel sensing materials because of their high surface area which enhances detective sensitivity, their specific structural features (open metal sites, tunable pore sizes, etc.) which promote host–guest interactions and selectivity, and flexible porosity which enables the reversible release and uptake of small target molecules [131,135,136].

Presently, the exploitation of MOFs' potentiality in gas sensing is affected by some limitations [135,137]: (1) Most pure MOFs are not stable under extreme conditions (high temperature and high humidity levels). (2) The types of gases detectable by MOFs are limited. (3) The inherent electrical conductivity of MOFs is low and this limits their use in the development of electronic sensors. (4) The interaction mechanism between MOFs and the analyte is poorly understood. (5) MOFs are generally produced as powders with a generally low mechanical strength and poor processability. This last limitation is particularly relevant since the sensitivity of gas sensors obtained from powders is low and poses the need for a post-process of MOFs as thin films or membranes.

To ensure the potential use of MOFs in sensing applications, most of these concerns must be addressed and, to this aim, the development of new MOF–based materials which have better properties (including processability in harsh conditions) than pure MOFs is gaining a lot of attention [137,138]. Research efforts have been focused on different strategies, including: (i) post-synthetic modifications [139]; (ii) linker change or functionalization; (iii) ion exchange; (iv) active groups grafting; (v) impregnation with suitable active materials; (vi) production of MOF-based hybrids/composites [126,138–140].

Among the different possibilities, the common adapted solutions are post-synthetic modifications and the production of hybrids/composites integrating MOFs and functional materials. Post-synthetic modifications involve the introduction of desired functional groups into the MOFs after their synthesis [126,139]. The modification can involve: the heterogeneous exchange of ligands or metal ions by breaking and forming chemical bonds within the original MOF, solvent-assisted ligand exchange, and replacement of the non-bridging ligands and metal nodes [123,139,141]. Mixed-metal MOFs, containing at least two metal ions in their framework, can be prepared under post-synthetic methods and

possess new properties and activities due to the presence of the second metal ion. This approach is frequently used to produce MOF-based materials exhibiting improved fluorescent/luminescent properties [139,141].

By combining MOFs with suitable materials, the functionality and the textural/thermal/magnetic/electric properties can be improved to meet specific requirements. In some cases, the hybrid/composite materials exhibit new properties that are superior to those of the individual components since they combine the advantages of both parent materials. Metal oxides [142], polymers [143], metal nanoparticles [144], silica [145], carbon nanotubes [146], graphene-related materials (GRMs) [140,147,148] and quantum dots [149] have been used for the production of MOF-based hybrids and composites [137,138].

A wide variety of methods have been applied for the preparation of MOF composites. The in situ growth approach involves the growth of MOF crystals under solvothermal/hydrothermal conditions in the presence of another functional material [138]. In this type of synthesis, the MOF structure is built from the precursors around and eventually inside the other composite component. This method has been mainly used for the preparation of MOF composites with carbon-based materials [140], metal oxides [150] or with metal nanoparticles [144,150]. During the synthesis, the second material can act also as a templating agent, leading to oriented growth of MOF crystals, and graphene is one such example [151]. In the encapsulation method, the MOF composite is formed starting from the second component precursors and the preformed MOF; namely, the second component forms inside the cages of the MOF and at the end of the synthesis, the particles stay stable inside the cages without directly bonding to the MOF structure [138]. This is the method primarily used for the production of MOF/polymer and MOF/NPs composites [138,143]. Solid grinding and impregnation are other strategies to incorporate NPs in MOFs [152,153]. The electrospinning and solution-blending methods are two possible approaches for the preparation of MOF/polymer membranes [150]. MOF composites for biomedical applications have been also produced by coating the MOF structure with silica or a specific polymer with the aim of reducing their cytotoxicity and intrinsic instability under physiological conditions [150].

The huge and wide variability in pore size distribution of MOFs allows different guest molecules with different characteristics (size, acid–base behavior, polarization, etc.) to easily access the cavity and interact with the pore surface due to the presence of unsaturated metal sites and Lewis acidic/basic sites [136,154]. In such a way, specific MOF properties can be influenced, and changes in optical, electrical, and mechanical MOF properties can occur [135,155]. On this basis, various MOFs have been developed for possible use as chemiresistive, magnetic, ferroelectric, colorimetric, as well as luminescent sensors [135,156,157]; many examples are reviewed in this section. The high porosity of MOFs and the easy reversibility of the interaction with the target guest molecule are valid prerequisites to achieve repeatability, regeneration and robust operability under repeated detection cycles. On the other side, signal transduction is a major challenge for the efficient utilization of MOFs in chemical sensing [136].

The sensitivity of MOF-based detection largely depends on the sensing method used for signal transduction. MOFs are generally coupled with such several signal transduction techniques and tools as chemiresistors, interferometry, quartz crystal microbalance (QCM), surface acoustic wave (SAW), and microcantilevers (MCLs). MOF-based thin-film techniques have hence been very recently suggested as a valid advantage for developing next-generation chemical sensors [157]. Moreover, recently, conductive MOFs have been synthesized by using proper organic ligands or doping with conductive materials to form hybrids and composites with the aim of generating detectable changes in resistance/capacitance upon guest-molecule exposure [158].

An overview of several different sensing mechanisms involving MOFs and the mainly detected gas types is provided in Figure 2 and detailed in the following sections.

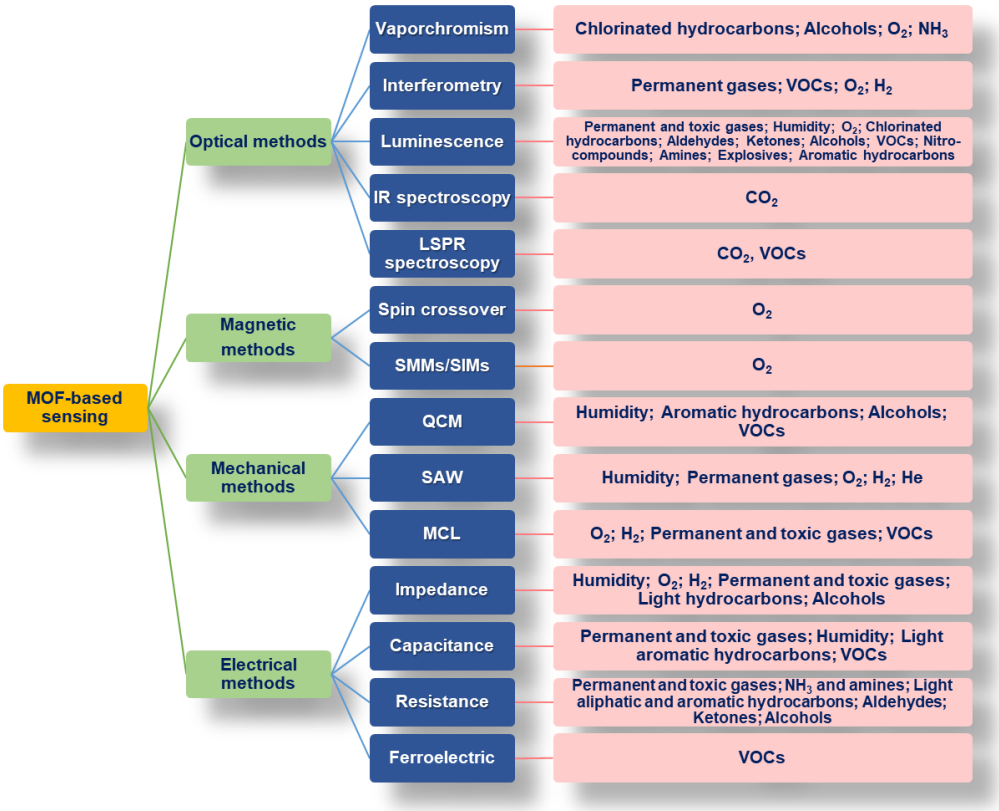

Figure 2. Scheme of the various methods employing MOF materials for chemical sensing.

4.2. MOFs in Optical Gas Sensing

When an analyte is adsorbed into the pores of a MOF, the interactions between guest and host may alter the charge transfer process between the ground and excited electronic states of the MOF constituents, in turn affecting their optical properties. In particular, changes in the material's color (i.e., changes in the absorption spectrum), in the luminescence intensity and/or spectrum and in the material's refractive index can occur due to interaction with the adsorbed gas. These changes can be used for gas sensing. We now consider some specific mechanisms upon which optical gas sensing by MOFs can be achieved:

4.2.1. Vapochromism

Vapochromism is based on shifts in the absorption spectrum caused by the electronic transition from the ground to the excited state of MOF chromophore components interacting with guest molecules. In some cases, when MOFs are exposed to gases or vapors with a strong coordination property, changes in the coordination environment of MOF metal centers can also result in a large absorption-spectrum shift. This type of signal transduction is of high significance because it is fast and facile and there is no need for instrumentation if the color change can be achieved selectively.

For example, Razavi et al. [159] (see Figure 3) proposed the MOF TMU-34 ([Zn(OBA)$(H_2DPT)_{0.5}$]·DMF) as a chemoswitchable MOF to detect chloroform, since after exposure to the chlorinated hydrocarbon, the dihydrotetrazine groups of the MOF conversed into tetrazine groups, allowing the yellow crystals of TMU-34 to turn pink (the color of O-TMU-34, namely the oxidized form).

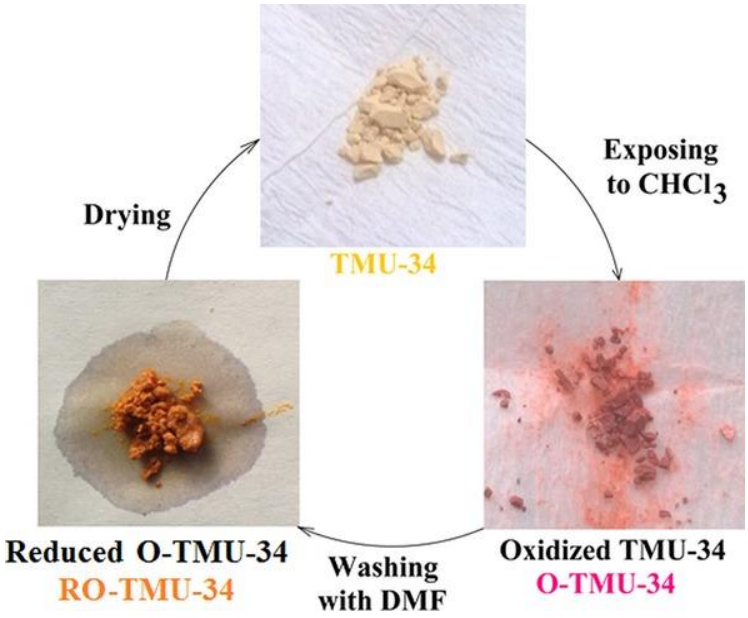

Figure 3. Sensing cycle for TMU-34, which is transformed, upon exposure to ChCl3, into O-TMU-34 which reverts back to TMU-34 after regenerating with DMF. Reprinted with permission from Ref [159], copyright 2017 John Wiley and Sons.

4.2.2. Luminescence

Several kinds of MOFs exhibit a significant luminescence efficiency, based on mechanisms which are schematically depicted in Figure 4 which mentions linker-based luminescence (ligand-localized emission), ligand-to-metal charge transfer (LMCT), metal-to-ligand charge transfer (MLCT), metal-based emission (including metal-to-metal charge transfer (MMCT)), and several others [157]. As a consequence, luminescence-based transduction is a scheme frequently employed in MOF-based chemical sensing. As previously mentioned, such a scheme relies on the amplification (enhancement) and/or quenching of the luminescence intensity induced by interactions between the adsorbed analyte and the luminophores of the MOF [136].

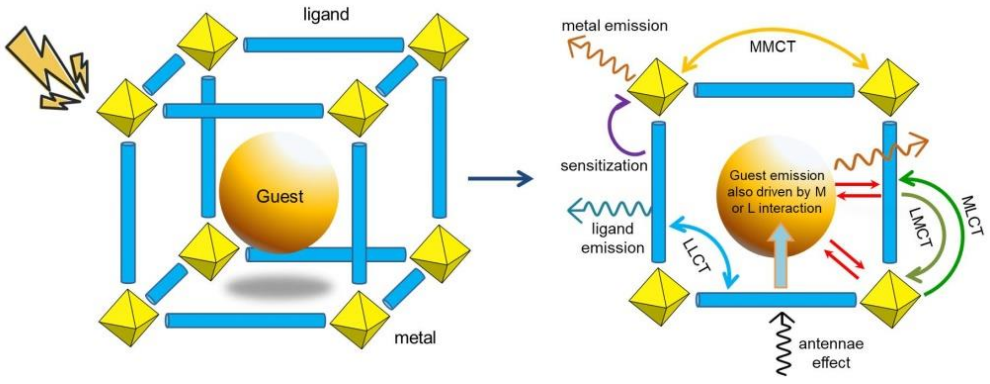

Figure 4. MOF-luminescence-based mechanisms of signal transduction.

The popularity of luminescence-based sensing resides in a combination of its technical simplicity, achievability of molecule-specific recognition and, in many cases, low limits of detection. It is also worth mentioning that the preparation of a luminescence-based sensing setup uses few components (i.e., an excitation source, an optical detector and optical components such as optical waveguides or optical fibers, allowing the propagation of the optical signal from the sample to the detector). Hence, it is often possible to assemble cost-effective and portable sensor devices [160].

Lanthanide-based MOFs, d^{10} metal-based MOFs containing functional ligands, heterometal–organic frameworks and MOFs incorporating fluorescent organic linkers have been tested for the detection of many analytes, including ions. Recent review articles have summarized the results regarding the use of luminescent-MOF-based sensors both for the detection of gaseous species and ions or molecules in solution [161–165].

4.2.3. Interferometry

The interferometry-based method measures the variations in the MOF refractive index (RI) before and after guest adsorption. Because most of the MOF volume is composed of initially vacant pores, the sorption of analytes inside these empty cavities leads to large RI increases [166]. This measurement requires the MOFs to be in thin-film form, and the reflective surfaces to be the front and back sides of the MOF film [136]. Another possibility is the development of gas-sensing MOF-based optical fibers optical-fiber-MOF-based by directly allowing the growth of a thin film of MOF on the surface of an optical fiber with controlled film thickness and morphology [166].

One of the first interferometric gas sensors implementing a MOF is the waveguide-based chemical-sensing platform based on ZIF-8-coated optical fiber for the detection of H_2, N_2, O_2, CO_2, and CO proposed by Kim et al. [167]. The ZIF-8-based sensor showed a high selectivity to CO_2 gas relative to other small gases (H_2, N_2, O_2, and CO) [167].

4.2.4. Localized Surface Plasmon Resonance (LSPR)

LSPR is a method similar to interferometry and detects analytes indirectly by measuring spectroscopically the RI changes in MOFs as shifts in the visible extinction spectrum. The sensor is based on a surface-sensitive measurement and, as a consequence, the thickness of the MOF films is the most important parameter for the development of a plasmonic sensor. MOF-based LSPR exhibits sensitivity and selectivity to different analytes since MOFs can selectively adsorb and concentrate specific analytes.

One of the first applications of MOF in gas-LSPR-based sensing was proposed by Kreno and coworkers [168]. They demonstrated amplifying the sensing signal by coating the plasmonic substrate with a MOF. Cu(BTC) was used as MOF structure and a 14-fold signal enhancement for CO_2 sensing was achieved [168]. Recently, also He and coworkers proposed the use of the same copper-based MOF in a tip-based fiber optic LSPR sensor for the sensing of VOCs [169].

4.2.5. Infrared Spectroscopy

Optical gas sensors using infrared (IR) absorption spectroscopy are mainly based on the modification of the intensity of transmitted and/or reflected light by the sensing material caused by gas adsorption [155,156]. While measurements of the transmitted wave determine the absorption coefficient of the sample, reflection-mode analysis can take advantage, in some specific cases, of the total internal reflection phenomenon [136].

4.3. MOF-Based Sensors Using Gravimetric and Mechanical Methods

The easier approach for gas detection utilizing MOFs is the measurement of changes in MOF mass as the material selectively adsorbs the target analyte. This can be performed on a macroscale, bulk scale, or by using thin films deposited on a mechanical resonator. In this last case, the change in mass of the resonator due to gas adsorption is translated into an electrical signal [154].

In these mechanical methods, at first, an analyte is adsorbed into the pores of MOFs grown on electromechanical devices and then the mass changes are converted into an electrical signal through different transduction mechanisms (shifts in frequency or changes in the work function) [154]. In this framework, an important aspect is related to the characteristics of the MOF films: a tight contact between the MOF film and the electromechanical-device surface is strictly required to obtain the suitable sensitivity.

The main gravimetric and mechanical methods involving MOFs for gas-sensing applications are based on the following electromechanical devices:

4.3.1. Quartz Crystal Microbalance (QCM)-Based Sensors

In QCM-based sensing, a thin piezoelectric quartz crystal is the core component of a QCM transducer [170]. After being electroplated, the thin slice oscillates when an alternating current (AC) is applied. The mass increases upon the adsorption of analyzed gas molecules, and the resonant frequency decreases (Figure 5) [170].

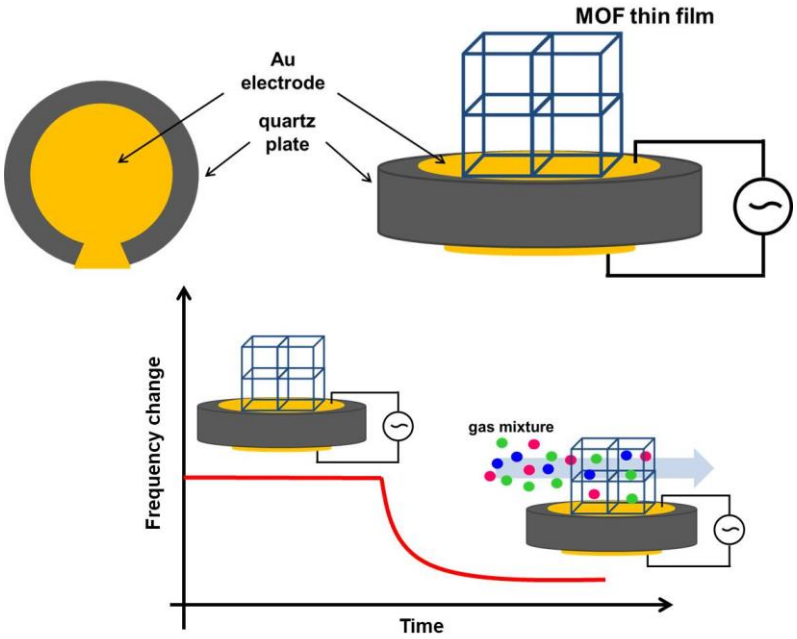

Figure 5. Scheme of MOF-based QCM gas sensor.

QCM-based MOF gas sensors have been successful in sensing a wide range of analytes using both reversible and irreversible interactions [155,171], even if little chemical identity or selectivity information can be directly obtained. QCM-based MOF sensors have been mainly proposed for humidity, VOC and hydrocarbon detection [155,171]. For example, Ma et al. used a MOF-based QCM gas sensor to detect inert and nonpolar gases such as BTEX (benzene, toluene, ethylbenzene, and xylene) [172]. To address the cross-sensitivity issue, QCM sensor arrays based on the combination of different MOFs to detect the same gas mixture have been recently proposed. Such a cross-sensitive sensor can be defined as an electronic nose (e-nose) [136].

4.3.2. Surface Acoustic Wave Sensors (SAWS)

In surface acoustic wave sensors (SAWS), the gas adsorption is detected by measuring the frequency shift of acoustic waves generated by a quartz oscillator vibrating and traveling parallel to the surface [173]. The response of this device is reproducible and faster as compared to the same coating on QCMs, but it is dependent on the film thickness: for each device, an optimal thickness can be estimated, above which the sensor response saturates [136]. Examples of MOF-based SAWS have been proposed by Paschke et al. (MOF@SAW sensor based on MFU-4 for the detection of H_2, N_2, CO_2) [174], Devkota et al. (ZIF-8-coated SAW reflective-delay-line mass sensors for the sensitive detection of CO_2 and CH_4 at ambient conditions) [175] and by Vanotti et al. (SAW device functionalized with ZnTACN for CO_2 detection) [176].

4.3.3. Microcantilever-Based Sensors (MCLs)

Gas detection by microcantilever (MCLs) sensors are characterized by two transduction mechanisms: the changes in the cantilever oscillation frequency caused by mass uptake and the strain-induced bending [177]. In the former mode, changes in the sensor oscillation frequency are typically detected optically. In the latter mode, adsorption produces strain at the coating's MCL interface, causing deflection of the cantilever beam that can be detected either optically or by using a built-in piezoresistive sensor. The structural flexibility of MOFs is an advantage for chemical detection using static MCL, because even small changes in the unit cell dimensions can result in large tensile or compressive stresses at the interface between the cantilever and the MOF thin film [160]. However, MCL-based sensors are scarce in practical applications, due to cross-sensitivity and poor selectivity; indeed, in the case of exposure to a gas mixture with multiple components, all constituents can be absorbed. Different kinds of MOFs have been proposed for the development of MCL-based gas sensors: UiO-66 for toxic organophosphorus molecules [178]; MIL-53 (Al) for CO_2, N_2, CO, and Ar [179]; and HKUST-1 for the detection of VOCs [180].

4.4. MOF-Based Sensors Using Electrical Methods

Electrical sensor devices based on MOFs detect a target gas by the changes in an electrical property among resistance, capacitance, impedance or work function.

4.4.1. Chemoresistors

As already mentioned, the working principle of chemiresistive gas sensors is based on the changes in electron conductivity (or resistance) of the sensitive layer/material as a consequence of the interaction with the target gas [48]. The origin of the chemiresistive effect in a MOF depends on its composition; redox reactions involving transition metals in MOFs can affect their conductivity, and structural changes or volume changes in MOFs upon gas adsorption modulate the number of electrons hopping between MOFs and thus cause resistance changes (Figure 6).

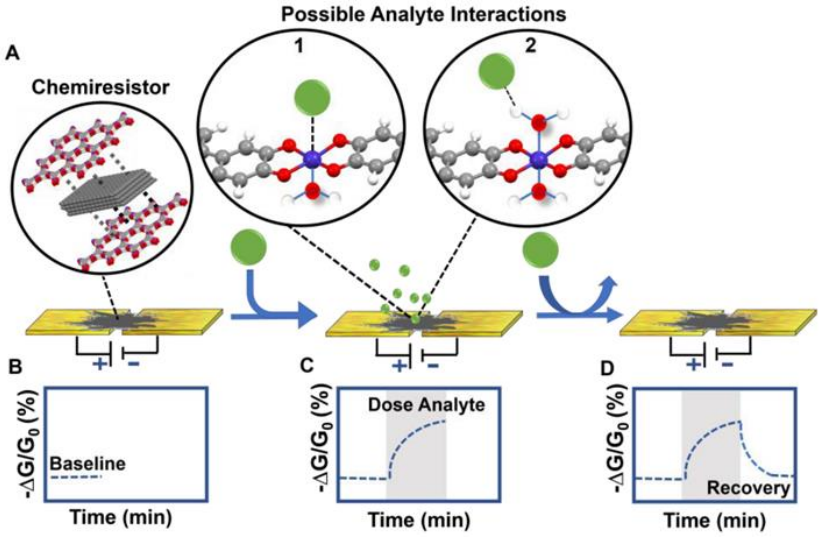

Figure 6. Chemiresistive—based MOF gas sensors sketch, reproduced from Ref. [181]. (**A**) the sensing layer completes a circuit by bridging two electrodes. (**B**) baseline. (**C**) The analyte (green circle) interacting with the sensing layer leads to a change in conductance coincident with analyte binding. (**D**) Recovery phase.

MOF-based chemiresistive sensors have been widely studied, as they offer a simple sensing mechanism, low-cost fabrication, facile integration with various electronic devices, and ease of miniaturization [48,135]. In addition, because of the diversity and high com-

patibility of MOFs and MOF derivatives with other materials, multiple principles can be incorporated for MOF-based chemiresistors [48].

The first MOF-based chemiresistive sensor was proposed by Chen et al. The authors constructed a Co-based ZIF-67 sensor for the detection of formaldehyde at concentrations below 5 ppm [182]. After this, many other works reported the development of MOF-based chemiresistive sensors implementing different kinds of MOFs and their results have been summarized in different review articles [48,135,183].

4.4.2. Chemicapacitive Sensors

The sensors belonging to this class probe the adsorption of a certain amount of target gas via changes in the relative permittivity (i.e., dielectric constant) of a sensing layer (usually a porous material). As MOFs benefit from insulating effects, they can be applied as dielectric layers in capacitance sensors [154].

Chemicapacitive sensors are mainly built up using two types of configurations—IDE (interdigitated electrode configuration) and the parallel plate configuration—differing in the geometry and in the positioning of the sensing layer (i.e., the MOF layer). In the former, the MOF material is deposited onto the electrodes, while in the latter, the MOF layer is collocated in a sandwich form between two metal substrates (usually copper plates), one employed as a back electrode and another as an upper electrode [154,183].

The signals of MOF-based chemicapacitive sensors (linked to changes in the permittivity of the MOF) are influenced by many factors: (i) the polarity of target molecules; (ii) the adsorbed amount of gas/vapor molecules on the sensing layer; (iii) structural features of target molecules affecting the size-exclusion-based selectivity, such as molar mass, chain length and kinetic diameter; (iv) the external environment conditions (temperature, relative humidity (RH), and frequency of measuring circuit).

Different examples of chemicapacitive MOF-based sensors have been proposed: (i) sensors with copper-based MOFs (HKUST-1 and Cu(bdc)xH_2O) have been used for the detection of humidity [184,185], (ii) sensors with yttrium-based MOFs have been used for the detection of toxic gases (NH_3 and H_2S) [186,187]; (iii) a sensor with HKUST-1 nanoparticles has been investigated for the detection of VOCs in a moderate environment [188].

4.4.3. Sensors Based on Changes in AC Impedance

The detection of changes in electrical impedance—namely, the quantity that generalizes the concept of resistance in the case of alternating currents—upon gas exposure is another approach for gas sensing. Since the electrical impedance changes as a function of the frequency of an applied sinusoidal voltage, the use of sensitive materials characterized by high conductivity is avoided and also highly resistive materials such as MOFs can be used for the development of gas sensors. Impedance measurements involving MOF-based systems depend on: (a) the uptake of the target analyte by the MOF-based sensing layer; (b) how the interaction between the MOF structure and guest molecules (adsorbed gas) facilitates efficient proton conduction; (c) the experimental conditions (temperature, RH, frequency of measurement, and concentration of the target analyte).

A variety of MOFs, such as Al-BDC MOF, Cu-BTC MOF, Fe-BTC MOF, Fe-doped Fe-BTC and Li-doped Fe-BTC MOFs, were tested for their impedimetric changes upon exposure to gases such as O_2, H_2, NO, CO_2, C_3H_8, ethanol and methanol [189]. Impedance-based sensors of humidity based on MOFs have been also developed; Weiss and coworkers proposed the use of different CAU-10 MOFs [190] while Y. Zhang et al. proposed the use of (Ti)MIL-125-NH_2 [191].

4.4.4. Sensors Based on Changes in the Work Function

The principle of work function readout exhibits potential for low-cost gas sensor development. A Kelvin probe is the technique to monitor work function changes. The changes in the work function are reflected as signal variation in the response of contact potential difference (CPD, $\Delta\varphi$) in the Kelvin probe transducer [192]. The surface electrode

modified with MOF adsorbs and concentrates the gas/vapor molecules, amplifying the response signal. The electrostatic interactions between gases and MOFs should lead to detectable changes in the work function (ΔΦ). The ability of MOFs for selective gas detection using work function readout (Kelvin probe measurements) has been demonstrated by the research activities of Davydovskaya and coworkers. In particular, they tested the use of Cu-BTC for aldehyde sensing [193], the suitability of different M–BTC-based MOFs (M = Co, Cd, Ni, Al) for alcohol and alkane sensing [193], and Mg-MOF74 and Co-MOF74 for CO_2 sensing [194].

4.5. Additional Methods

Additional transduction schemes for chemical detection which can involve ferroelectric or magnetic properties are also briefly mentioned here.

4.5.1. Methods Involving Ferroelectric Properties

Ferroelectric properties can be involved when the positive and negative charge centers of the MOF crystal do not coincide, so that an intrinsic electric dipole moment and a spontaneous macroscopic polarization arise. The ferroelectric properties of MOFs mainly derive from the hydrogen bond interactions of MOFs and polar guest molecules, which endow them with ferroelectric properties [195]. MOFs can be used as ferroelectric switch materials due to their sensitivity to external stimuli, but such an application is still in the initial stage of development [135]. This limited development is because the MOFs used as ferroelectric switches must meet two stringent conditions: (1) the space groups of the MOF must belong to polar point groups; (2) the MOF should have a hydrophilic cavity. In addition, the measurement of ferroelectric properties requires large-scale single crystals, but MOFs are not easily produced as large-scale crystals.

4.5.2. Methods Involving Magnetic Properties

Magnetic-MOF-based sensing switches are mainly produced from two types of magnetic MOFs: (i) spin crossover (SCO) MOFs and (ii) single-molecule magnet/single-ion magnet (SMMs/SIMs) MOFs [135]. Their magnetic behaviors (such as magnetic ordering, magnetic susceptibility, hysteresis loop, spin crossover, etc.) can be easily modulated through the single-crystal-to-single-crystal (SCSC) transformation, which occurs with the exchange of the guest solvent molecules or cleavage and formation of chemical bonds, that in turn modulates the magnetic properties. The metal centers of SCO MOFs are common transition metal ions with d^4–d^7 electronic configurations, as these metal ions may exist in high-spin (HS) and low-spin (LS) states, while SMMs/SIMs MOFs are composed of d- and f-block (Mn^{2+}, Fe^{2+}, Dy^{3+}, etc.) metal complexes [135].

MOF-based magnetic switches are still rare, particularly in combination with other properties. As a first work on the topic, Han et al. proposed a magnetic-MOF-based oxygen sensor based on Fe-MOF-74 to investigate the relationship between the O_2 absorption and MOF magnetic properties [196].

4.6. Recent Advances in Gas Sensing Based on MOF-Based Hybrid Organic–Inorganic Composites

The recent literature results regarding the use of MOF-based hybrid composites have been analyzed and summarized in the following table. The reason why the Table focuses only on MOF-based composites is twofold. First, the literature about gas-sensing applications of pure MOF structures is extremely vast, as can be seen by reading some recently published, relevant review papers [197–200]. We hence decided to avoid discussing pure MOFs and focused on a specific subclass. Moreover, and probably even more importantly, the synthesis and application of MOF-based composites are nowadays considered hot research topics, in which scientists and technologists are pursuing their goals by taking advantage of the combined functionality of both the metal–organic and the organic/inorganic components of the composite.

In Tables 3 and 4, we propose a vast survey of gas-sensing literature works centered on the use of MOF-based composites and published in recent years (from 2016 to now). As most of these composites are successfully employed as chemiresistors, we decided to split the two separate approaches: Table 3 shows data regarding only the works where the composite material is used as a chemiresistive sensor, while Table 4 deals with other transduction approaches/mechanisms.

As can be guessed, a relevant class of materials suitable for the synthesis of gas-sensitive composites based on MOFs are MOXs (metal oxides) which, as previously mentioned, exhibit several advantages but also some important drawbacks, such as poor selectivity and cross-sensitivity to humidity. Moreover, metal oxide chemiresistors operate at high temperatures (200–600 °C), which make them unsuitable for some real-life applications. Similar arguments can be made for carbon-based materials: they are interesting for gas-sensing applications and exhibit a large specific surface area, but also have problems with selectivity and often exhibit low reproducibility. To address these issues, the idea of developing composite materials compounding these sensing materials with MOFs to obtain a synergistic effect aimed at improving the overall gas-sensing performance has been recently formulated [137].

MOFs-MOXs hybrid composites may offer physicochemical properties not achievable by parent MOFs and are expected to exert outstanding advantages since the MOF component typically retains most of its large surface area, high porosity, and property tunability, gaining stability and conductivity thanks to the filler inclusion. In addition, the unique gas storage and gas selectivity properties of MOFs can improve the selectivity of the resulting composite. According to this trend, the use of MOF membranes on metal oxides is being explored as an approach for enhancing the sensor selectivity [137].

Table 3. Literature results regarding use of MOF-based composites as chemiresistive gas sensors. Response, as defined in the table, is mentioned when available for a specific value of the analyte concentrations and/or for a range of values. Unless stated otherwise, the letters R, I and G are used to indicate the electrical resistance, the current intensity and the conductance, while the suffix "0" and "g" refer to the values of one of such quantities measured in air (i.e., without an analyte) and in the presence of the gas analyte. $\Delta R = |R_g - R_0|$; ΔI and ΔG hence indicate the gas-induced change in resistance, current intensity and electrical conductance, respectively.

Analyte	Material	T (°C)	Conc.	Response	Ref
H_2					
	ZnO@ZIF-8	300	50 ppm	1.44 (R_0/R_g)	[201]
	ZnO@ZIF-8	250	50 ppm	3.28 (R_0/R_g)	[202]
	ZnO@ZIF-8	125	10 ppm	~5 (R_0/R_g)	[203]
	ZnO@ZIF-8	250	50 ppm	~80% ($\Delta I/I_0$)	[204]
	ZnO@ZIF-71	250	50 ppm	~80% ($\Delta I/I_0$)	[204]
	Pd nanowires@ZIF-8 (4 h)	RT	0.1%	0.7% ($\Delta R/R_0$)	[205]
	ZnO@Pd@ZIF-8 nanowires	200	50 ppm	6.6 (R_0/R_g)	[206]
	Pd NWs@rGO@ZIF-8	RT	100 ppm	2.2% ($\Delta R/R_0$)	[207]
	ZnO@ZIF-8	290	1000 ppm	~6 (R_0/R_g)	[208]
	MOF-5/CS/IL	RT	100 ppm	~0.1 (R_0/R_g)	[209]
	Pd/ZIF-67	RT	3000 ppm	9% ($\Delta I/I_0$)	[210]
	Pd/ZIF-67/PMMA	RT	3000 ppm	7% ($\Delta I/I_0$)	[210]
	HKUST-1/Pd NP/SWCNT	N.A.	10 ppm	(not defined)	[211]
CO_2	SnO_2@ZIF-67	205	5000 ppm	16% ($\Delta R/R_0$)	[212]
	GA@UiO-66-NH_2	200	5% to 100%	2% to 8% ($\Delta R/R_0$)	[213]
NO_2					
	In_2O_3/ZIF-8 (4:1)	140	1 ppm	16.4 (R_g/R_0)	[214]
	$Cu_3(HHTP)_2/Fe_2O_3$	RT	5 ppm	63% ($\Delta R/R_0$)	[215]
	Pd@$Cu_3(HHTP)_2$	RT	5 ppm	62% ($\Delta R/R_0$)	[216]
	Pt@$Cu_3(HHTP)_2$	RT	5 ppm	57% ($\Delta R/R_0$)	[216]
	Pt@$Cu_3(HHTP)_2$	RT	3 ppm	90% ($\Delta R/R_0$)	[217]
	ZnCo-ZIF/graphene nanoplatelets	22 °C, 30% RH	100 ppm	~30 (R_0/Rg)	[218]
	MIL-101(Cr)-PEDOT(45)	RT	1 ppm to 10 ppm	1–30 ($\Delta G/G_0$)	[219]

Table 3. *Cont.*

Analyte	Material	T (°C)	Conc.	Response	Ref
H_2S					
	MOF-5/CS/IL	RT	100 ppm	0.91 (R_0/R_g)	[209]
	WO_3@ZIF-71	250	20 ppm	19% ($\Delta R/R_0$)	[220]
	ZIF-8/ZnO	25	10 ppm	52% ($\Delta R/R_0$)	[221]
	Co-Zn-MOF@CNT	325	100 ppm	~60 (R_g/R_0)	[222]
NH_3					
	ZnO@ZIF-8	250	50 ppm	~25% ($\Delta I/I_0$)	[204]
	ZnO@ZIF-71	250	50 ppm	~25% ($\Delta I/I_0$)	[204]
	Cu-BTC/GO (25)	RT	500 ppm	7% ($\Delta R/R_0$)	[223]
	Cu-BTC/PPy-rGO	25, 50% RH	50 ppm	12.4% ($\Delta R/R_0$)	[224]
	Pd-Co@IRMOF1	RT	90 ppm	~80 (R_0/R_g)	[225]
	SiO_2CuOF-graphene-PAni	N.A.	200 ppm	150% ($\Delta R/R_0$)	[226]
	ZIF-67/rGO	rt	50 ppm	5.8 (R_0/R_g)	[227]
	ZIF-8@ZnO porous nanospheres	220	50 ppm	~6 (R_0/R_g)	[228]
	ZnCo-ZIF/graphene nanoplatelets	25, 30% RH	1000 ppm	~1.1 (R_0/R_g)	[218]
	$Cu_3(HHTP)_2$/graphite	RT	80 ppm	5% ($\Delta G/G_0$)	[181]
	$Co_3(HHTP)_2$/graphite	RT	80 ppm	4% ($\Delta G/G_0$)	[181]
	$Fe_3(HHTP)_2$/graphite	RT	80 ppm	4% ($\Delta G/G_0$)	[181]
	$Ni_3(HHTP)_2$/graphite	RT	80 ppm	3% ($\Delta G/G_0$)	[181]
CO					
	MOF-5/CS/IL	RT	100 ppm	~8% (R_0/R_g)	[209]
	ZnCo-ZIF/graphene nanoplatelets	22, 30% RH	1000 ppm	~1.4 (R_0/R_g)	[218]
CH_4					
	ZnCo-ZIF/graphene nanoplatelets	22, 30% RH	1000 ppm	~1.5 (R_0/R_g)	[218]
NO					
	$Cu_3(HHTP)_2$/graphite	RT	80 ppm	8% ($\Delta G/G_0$)	[181]
	$Fe_3(HHTP)_2$/graphite	RT	80 ppm	11% ($\Delta G/G_0$)	[181]
	$Ni_3(HHTP)_2$/graphite	RT	80 ppm	10% ($\Delta G/G_0$)	[181]
H_2O					
	Matrimid-NH_2-MIL-53(Al)	28	2%	12% ($\Delta G/G_0$)	[229]
	ZIF-8/MWCNT	25; 20% RH	100 ppm	11% ($\Delta R/R_0$)	[230]
	ZIF-8/MWCNTs/AgNPs	RT	1%	2.5% ($\Delta R/R_0$)	[231]
CH_2O (Formaldehyde)					
	ZnO@ZIF-8	300, 10% RH	100 ppm	~13.5 (R_0/R_g)	[232]
	ZnO@ZIF-8	RT	5 ppm to 100 ppm	7 to 210 (R_0/R_g)	[233]
	Janus Au@ZnO@ZIF-8	25	50 ppm	5–20 (R_0/R_g, sample dependent)	[234]
	ZIF-8/MWCNT	25; 20% RH	100 ppm	200% ($\Delta R/R_0$)	[230]
	ZIF-8@ZnO porous nanospheres	220	50 ppm	~9.7 (R_0/R_g)	[228]
	Pd-Co@IRMOF1	RT	90 ppm	~10 (R_0/R_g)	[225]
CH_3COCH_3 (Acetone)					
	ZnO@5nmZIF-CoZn	260	10 ppm	28 (R_0/R_g)	[235]
	ZnO@ZIF-8	250	50 ppm	~20% ($\Delta I/I_0$)	[204]
	ZnO@ZIF-71	250	50 ppm	~240% ($\Delta I/I_0$)	[204]
	ZnO@ZIF-71	150	5 ppm	39% ($\Delta I/I_0$)	[236]
	ZIF-8/MWCNTs/Ag NPs	rt	1%	2.3% ($\Delta R/R_0$)	[231]
	ZIF-8/MWCNT	25; 20% RH	100 ppm	4.6% ($\Delta R/R_0$)	[230]
	ZnO@ZIF-8	290	50 ppm	~2 (R_0/R_g)	[208]
	ZIF-8@ZnO porous nanospheres	220	50 ppm	~8 (R_0/R_g)	[228]
	Pd-Co@IRMOF1	RT	90 ppm	~8 (R_0/R_g)	[225]
	Pd/ZIF-67	RT	3000 ppm	0.5% ($\Delta I/I_0$)	[210]

Table 3. *Cont.*

Analyte	Material	T (°C)	Conc.	Response	Ref
CH_3CH_2OH (Ethanol)					
	ZnO@ZIF-8	250	50 ppm	~40% ($\Delta I/I_0$)	[203]
	ZnO@ZIF-71	250	50 ppm	~325% ($\Delta I/I_0$)	[203]
	ZnO@ZIF-71	150	10 ppm	13.4% ($\Delta I/I_0$)	[236]
	ZIF-8/MWCNTs/Ag NPs	RT	1%	12% ($\Delta R/Ra$)	[231]
	ZnO@ZIF-71@PDMS	250	10 ppm	500% ($\Delta I/I_0$)	[237]
	Matrimid-NH_2-MIL-53(Al)	28	2%	~8% ($\Delta G/G_0$)	[229]
	ZIF-8/MWCNT	25; 20% RH	100 ppm	26.4% ($\Delta R/R_0$)	[230]
	ZnO@ZIF-8	290	100 ppm	~2 (R_0/R_g)	[208]
	ZIF-8@ZnO porous nanospheres	220	50 ppm	13.8 (R_0/R_g)	[228]
	Pd-Co@IRMOF1	RT	90 ppm	20 (R_0/R_g)	[225]
CH_3OH (Methanol)					
	ZIF-8/MWCNTs/Ag NPs	RT	1%	8% ($\Delta R/R_0$)	[231]
	Matrimid-NH_2-MIL-53(Al)	28	20,000 ppm	8% ($\Delta G/G_0$)	[229]
	ZIF-8/MWCNT	25–27, 20% RH	100 ppm	20% ($\Delta R/R_0$)	[230]
	ZIF-8@ZnO porous nanospheres	220	50 ppm	8 (R_0/R_g)	[228]
	$Cu_3(HHTP)_2$/graphite	RT	500 ppm	2% ($\Delta G/G_0$)	[181]
	SnS/ZIF-8	25	10 ppm	~60 ($\Delta G/G_0$)	[238]
C_2H_4 (ethene)	ZnO@ZIF-8	350 °C, 25% RH	250 ppm	20% ($\Delta G/G_0$)	[239]
C_3H_6 (propene)	ZnO@ZIF-8	350 °C, 25% RH	250 ppm	60% ($\Delta G/G_0$)	[239]

Table 4. References on the use MOF-based composites as gas sensors employing methods different from the chemiresistive one. Unless stated otherwise, all the data refer to experiments performed at room temperature. The response for Ref [234] is defined as the minimal motional resistance change. QCM and PL stand for quartz crystal microbalance and photoluminescence, respectively. The transduction parameter is the ratio of optical transmittances (I/I_0) as measured with and without the analyte, respectively. In the case of the QCM sensor, the response is defined as the relative shift in the resonance frequency $\Delta f/f$. In the case of the PL-based transduction, the response is defined as the ratio between the luminescence intensities at a responsive wavelength or as the ratio between PL intensity in the presence of the analyte (I) divided by the PL intensity in the absence of the analyte (I_0).

Analyte	Method	Material	Conc.	Response	Ref.
CH_4	Optical-fiber transmittance	ZIF8/PDMS	20% to 50% (in N_2)	1.05–1.15 (I/I_0)	[240]
CH_4	Optical-fiber transmittance	SBS/Fe(Pyz)Ni$(CN)_4$ (50%)	100% to 20%	Little % transmittance	[241]
CO_2	Optical-fiber transmittance	SBS/Fe(Pyz)Ni$(CN)_4$ (50%)	100% to 10%	Little % transmittance	[241]
CO_2	Optical-fiber transmittance	PMMA/ZIF-8	0% to 100%	Up to 30% transmittance reduction	[242]
CO_2	Interference fringe shift in cavity	ZIF8-decorated WGM microcavity	25% to 100%	$\Delta\lambda = 7.4$ pm per % of CO_2 concentration	[243]
CO_2	IR absorption	Plasmonic nanopatch array-ZIF-8	20% to 35%	~4×10^2 (enhancement factor of the IR absorption)	[244]
NH_3	Optical	MIL-124@Eu^{3+}/Al_2O_3	500 ppm	14% ($\Delta I/I_0$)	[245]
NH_3	QCM	TiO_2-SnO_2/MWCNTs@Cu-BTC	40 ppm	0.8, see table caption for the definition	[246]

Table 4. *Cont.*

Analyte	Method	Material	Conc.	Response	Ref.
H_2O	QCM	CNT-HKUST-1	5% to 75% RH	2.5×10^{-5} of ($\Delta f/f$) per percent of humidity	[247]
CH_2O	PL	Eu(III)-functionalized ZnO@MOF	10 ppm	5.5, defined as I (614 nm)/I (470 nm)	[248]
C_6H_6	PL	Eu(III)-functionalized ZnO@MOF	10 ppm	2.4, defined as I (614 nm)/I (470 nm)	[248]
Ethyl-benzene	PL	Eu(III)-functionalized ZnO@MOF	10 ppm	2.4, defined as above	[248]
Toluene	PL	Eu(III)-functionalized ZnO@MOF	10 ppm	2.3, defined as above	[248]
Nitrobenzene	PL	$[Ca(H_2EBTC)(DMF)_2]$@PVDF	50 ppm	1.3 (I_0/I)	[249]

Apart from MOXs, other classes of materials have been explored for achieving functional MOF-based composites; recently published works discuss, for example, the composition of MOFs with metal nanoparticles [142,144], carbon-based materials [140,146–149] and polymers [143].

4.6.1. Composites of MOFs with Metal Oxides (MOXs)

MOFs-MOXs composite structures designed and tested as gas sensors have up to now been tested mainly based on ZnO as the metal oxide (a smaller number of relevant works propose the use of other oxides) and of materials belonging to the family of zeolite imidazolate frameworks (ZIFs) as MOFs. ZIFs show a structure similar to zeolites. By changing the metal ion or organic ligand, ZIFs' gas-sieving ability can be easily tuned to improve the controllable sensor selectivity. In addition, ZIFs often exhibit hydrophobic properties [250]. During the production of MOF-MOX composites, MOX is used as a metal-ion source; indeed, the metal cations released in solution through MOX partial dissolution interact with organic ligands generating the desired MOF materials with the MOX anchored inside. This approach has been used mostly for the production of ZnO/ZIF composites [137].

ZnO/ZIF composites have been proposed as a sensing layer for the development of sensors for the detection of small gas molecules and VOCs (see Table 3). In such a structure, ZIFs act as a sieving material to concentrate the analyte before the interaction with ZnO. Drobek et al. [201] developed a sensor for H_2 detection by using ZnO nanowires encapsulated in the ZIF-8 structure, achieving improved selectivity for H_2 over C_7H_8 and C_6H_6 at 300 °C thanks to the sieving effect of ZIF-8.

ZnO/ZIF composites have been also proposed by Zhou et al. [204] for the detection of H_2, NH_3 and a selection of VOCs (ethanol, acetone and benzene). In particular, two ZIFs (ZIF-8 and ZIF-71) differing in pore sizes (∼3.4 Å for ZIF-8 and ∼4.8 Å for ZIF-71) were grown on the surface of ZnO nanorods to form ZnO@ZIF core–shell structures, where ZIFs act as a, gas-molecule-sieving layer to shield ZnO from other gas molecules different from the analytes and, thus, to improve the overall sensing selectivity. As a matter of fact, the sensor based on ZnO@ZIF-8 exhibited a better response to smaller molecules, i.e., to H_2 and NH_3, while the one based on ZnO@ZIF-71 was able to discriminate benzene, most likely as it has the largest molecular size among the three tested compounds (Figure 7). These results demonstrated that the selectivity of sensors based on ZnO can be, to some extent, controlled by tuning the structural properties of MOF coatings.

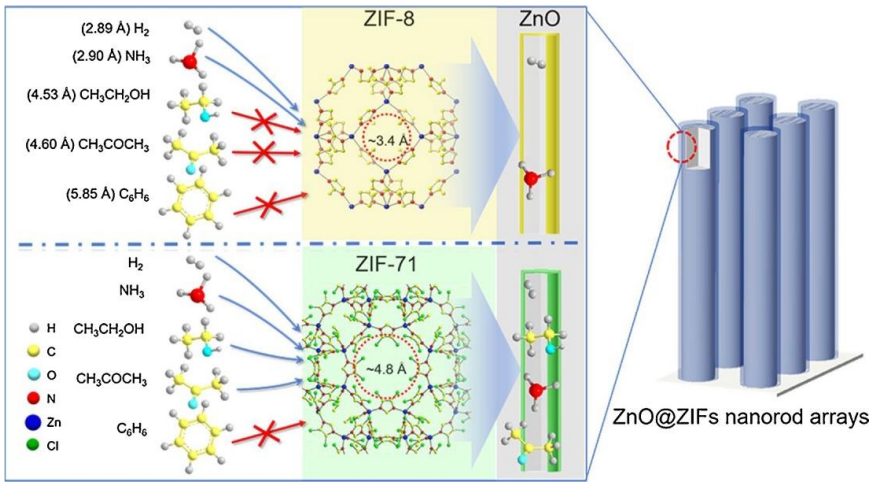

Figure 7. Sieving effect of ZIF-8 and ZIF-71 in ZnO@ZIF NRAs. Reprinted with permission from Ref. [204], copyright 2018 Elsevier.

The ability of ZIF-8 to concentrate the analyte by a sieving effect before the interaction with ZnO nanorods was demonstrated also by Tian et al. [232], who produced a highly selective formaldehyde gas sensor based on ZnO nanowires coated with ZIF-8.

Other studies also demonstrated that the thickness of the MOF layer—or, more generally, the amount of loaded MOF—affects the gas-sensing performance of MOF-MOX composites. Indeed, to increase the specific surface area of the sensing layer without increasing the diffusion path of the gas, an optimized shell layer thickness is needed. Wu et al. [202] obtained improved H_2 detection results by simply decreasing the MOF loading in the composite; indeed, the sensor with a complete ZnO@ZIF-8 core–shell structure experienced a higher hindrance of diffusion of the target gas to the ZnO. Additionally, Cui and coworkers obtained an improved response to H_2, also lowering the operating temperature to 125 °C by increasing the number of pure ZnO nanorods and decreasing the proportion of insulating ZIF [203].

Some modifications of the ZnO@MOF structure were also proposed. Yao and coworkers [235] added Co^{2+} ions to the synthesis mixture, preparing ZnO@ZIF-CoZn characterized by a higher selectivity for acetone and improved resistance to humidity compared to ZnO@ZIF-8. In the proposed composite, ZIF-CoZn acted as a filtration layer against water molecules, allowing a humidity-independent acetone-sensing behavior at 260 °C. The same authors synthesized an Au-ZnO@ZIF-DMBIM composite by partially replacing the 2-MIM ligand with DMBIM [251]. After the exchange of ligands, no changes in the material crystal structure occurred, but the pore size was reduced and, as a consequence, the absorption of benzene derivatives was further inhibited by the sieving effect, and the moisture resistance was improved.

Regarding the use of composites involving MOX different from ZnO, Dmello et al. [212] synthesized SnO_2-nanoparticle-encapsulated ZIF-67 (SnO_2@ZIF-67) to take advantage of the selective sorption properties of ZIF-67 towards CO_2. The composite exhibited a CO_2 response approximately 2-fold higher than that of pristine SnO_2 nanoparticles ($\Delta R/R_a$ = 8.8%). Zhou and coworkers proposed a WO_3@ZIF-71 composite for the development of a sensor with improved selectivity and response to H_2S [220]. They showed that the synthesized WO_3@ZIF-71 exhibited, compared to pure WO_3, an almost 9-fold-improved response.

Liu et al. synthesized In_2O_3@ZIF-8 heterostructures and used them for the development of a chemiresistive NO_2 sensor [214]. During the preparation of the heterostructures, ZIF-8 nanocrystals were uniformly deposited on In_2O_3 by using In_2O_3/ZnO as the source of zinc ions for the growth of ZIF-8. The optimized In_2O_3/ZIF-8 heterostructure exhibited at 140 °C a high response to 1 ppm NO_2 and an enhanced humidity resistance thanks to the hydrophobic ZIF-8 shield compared to the parent In_2O_3 (Rg/Ra = 4.9).

Zhang and coworkers synthetized a luminescent MIL-124@Eu^{3+} film on porous Al_2O_3 for the development of a NH_3-sensing system [245]. MIL-124 was allowed to grow on α-Al_2O_3 via in situ solvothermal synthesis; then, the doping with europium ions was carried out via a post-synthetic modification. The authors demonstrated that the luminescent intensity of the MIL-124@Eu^{3+} film exhibited an excellent linear relationship with NH_3 concentration in ambient air, reaching a detection limit as low as 26.2 ppm.

4.6.2. Composites of MOFs with Noble-Metal Nanoparticles

Composites with noble-metal nanoparticles (Pd, Pt, Au, and Ag) have been studied mainly for the purpose of H_2 detection. The ability of Pd nanoparticles to serve the detection of H_2 is based on changes in the resistance of the Pd-based sensor driven by the generation of palladium hydride (PdH_x) after the interaction between Pd and H_2 [48]. On the basis of this property, Koo et al. synthesized a Pd NWs@ZIF-8 composite in which ZIF-8 was directly grown on the Pd nanowires [205]. The ZIF-8 acted as sieving layer, allowing a selective penetration of H_2 in the Pd-based sensors and, hence, preventing the detrimental interaction between O_2 and Pd nanowires.

Kumar et al. proposed a H_2 sensor, using as a sensing layer ultrathin reduced graphene oxide (rGO)-coated palladium nanowires (Pd NWs@rGO) with a coating of ZIF-8 (Pd NWs@rGO@ZIF-8) [207]. The role of ZIF-8 was that of a nanofiltration layer; Pd NWs promoted a rapid response and high sensitivity towards H_2, while rGO prevented the formation of additional conductive channels due to the expansion of Pd NWs upon H_2 exposure, ensuring monotonic sensor response (Figure 8). The optimized device showed a response of 2% to 1% H_2 in air and a response time of 5 s and a lower limit of detection of 20 ppm. The same Pd NWs@rGO@ZIF-8 composite was also tested as a CO and CH_4 sensor, as reported in Table 3.

Xie and coworkers [210] proposed a H_2 sensor which used as a sensing element a composite consisting of a Pd nanocluster film, a ZIF-67 MOF, and a polymer (PMMA). The polymer coating acted as a protection layer ensuring resistance to CO poisoning and improving the sensitivity of the device to H_2. The MOF served as an interface layer between the Pd film and the polymer layer, leading to a significant improvement in the sensing performance. Compared with traditional Pd-based electric-conductance-type H_2 sensors, the proposed sensor exhibited optimized sensing capabilities.

Pd- and Pt-based composites have been proposed also for the detection of other small gases different from H_2, including VOCs. Koo et al. [216] published the results of a study involving a sensor based on composites of 2,3,6,7,10,11-hexahydroxytriphenylene hydrate (HHTP)-based MOF with Pd and Pt for the detection of NO_2, while a Pd/ZIF-67 composite was recently proposed for acetone and benzene detection by Xie and coworkers [210]. The detection of ethanol, acetone, formaldehyde and NH_3 was investigated by Khan and coworkers using Pd-Co/IRMOF composites [225].

Other composites involving noble metals employ the plasmonic properties of Au and Ag nanoparticles to enhance the response of optochemical sensor devices [144]. Wang et al. [234] coated the surface of Au nanorods with ZnO to form an Au@ZnO core–shell structure; then, ZIF-8 crystals were allowed to grow on the ZnO surfaces. ZnO in the resulting multilayered composite acted as an active-sensing material, while ZIF-8 acted as a sieve for formaldehyde and as hydrophobic protection for humidity. Finally, Au nanorods conferred a localized plasmonic resonance in visible light, so that at resonant illumination, resulting in an improved generation of free carriers in the ZnO surface, thus lowering the energy required for the device functioning and improving the response.

Chong et al. developed a nanophotonic device based on a plasmonic nanopatch array (NPA)@ZIF-8 composite for enhanced-infrared-absorption CO_2 sensing [244]. The collected experimental results showed that the proposed plasmonic-MOF-based device can effectively increase the infrared absorption path of on-chip gas sensors by more than 1100-fold. These results pave the way for the future development of on-chip gas sensing with ultracompact size.

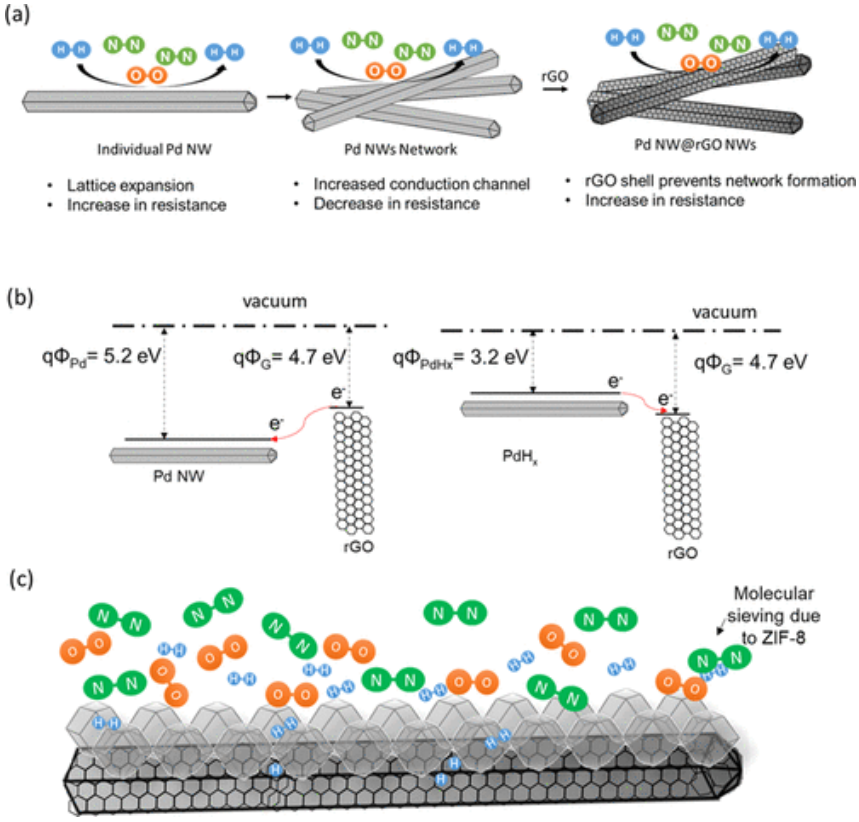

Figure 8. Pd NWs@rGO@ZIF−8 composite. (**a**) Sensing mechanism; (**b**) energy band diagram of Pd NW and p-type rGO, and PdH_x and p-type rGO; (**c**) molecular−sieving effect of ZIF−8 in the Pd NWs@rGO@ZIF−8 H_2 sensor. Reprinted with permission from Ref. [215]. Copyright 2021 American Chemical Society.

4.6.3. Composites of MOFs with Carbon-Based Materials

Carbon nanotubes (CNTs) and graphene-based materials (GRMs including graphene, graphene oxide, reduced graphene oxide (rGO), aminated graphene oxide, etc.) are the most common carbon-based materials reported in the literature that can be used for gas-sensing and gas adsorption applications, but they exhibit limited selectivity and low adsorption capacity for gases [252–256]. Their poor selectivity towards specific gases can be enhanced by compounding with MOFs, thus exploiting MOF as molecular sieves. In addition, the integration with carbon-based materials leads to an improvement in the stability and the electrical conductivity of the MOF structure [148]. Carbon-based MOFs proposed so far for sensing applications are based on a few MOF types: BTC-based MOFs, MOF-5, ZIF-8, and HTTP-based MOFs, as reported in Table 3. In all the cases, improved sensing performance, with respect to single components, was achieved.

Jafari et al. [231] synthesized a composite made up by ZIF-8, MWCNTs and Ag nanoparticles and they used it to develop a sensor for the detection of some VOCs including methanol, ethanol, acetone, acetonitrile and n-hexane at room temperature. Thanks to the ZIF-8-sieving properties, the proposed sensor exhibited good sensitivity to the analytes and higher sensitivities towards ethanol and methanol, namely, the two analytes smaller in size among the tested pool. Similarly, a trimetallic bilayer composite (Zn-Co-Ni MOF@CNT) was discussed by Tan et al. [222] for H_2S sensing, comparing its performances with those of a monolayer, bimetallic Zn-Co MOF@CNT composite.

Composites with carbon nanotubes were implemented also in the development of QCM-based sensors. Wong et al. [246] developed QCM-based sensors for NH_3 detection under ambient conditions covering the QCM quartz plate with a TiO_2-SnO_2/MWCNTs@Cu-BTC composite. In such a material, the presence of a TiO_2–SnO_2/MWCNT hybrid prevents

HKUST-1 decomposition, improving its longevity. The proposed QCM sensor exhibited a NH_3 limit of detection as low as 0.77 ppm and improved sensitivity, repeatability, good chemical selectivity for ammonia and stability, even in the presence of moisture. Chappanda and coworkers [247] proposed QCM-based humidity sensors based on HKUST-1/CNT thin films. The optimized sensing film demonstrated a 230% increase in sensitivity compared to a plain HKUST-1 film, stability, reliability, and an average sensitivity up to ten times better than previously reported.

In some examples, the MOF represents the conductive component, such as in the work by Ko et al. [181], who described the sensing performances of chemiresistive sensors based on using conductive MOF composites as sensing layers. The conductive MOFs were obtained by the integration of the MOF M_3HHTP_2 (M = Fe, Co, Ni, or Cu) with graphite by a solvent-free ball-milling procedure. The as-prepared chemiresistors were capable of detecting and differentiating NH_3, H_2S and NO at ppm levels (Figure 9). Other interesting results involving metal-doped MOFs are reported in Table 3 with reference to the detection of NO_2 [216] and NH_3 [225].

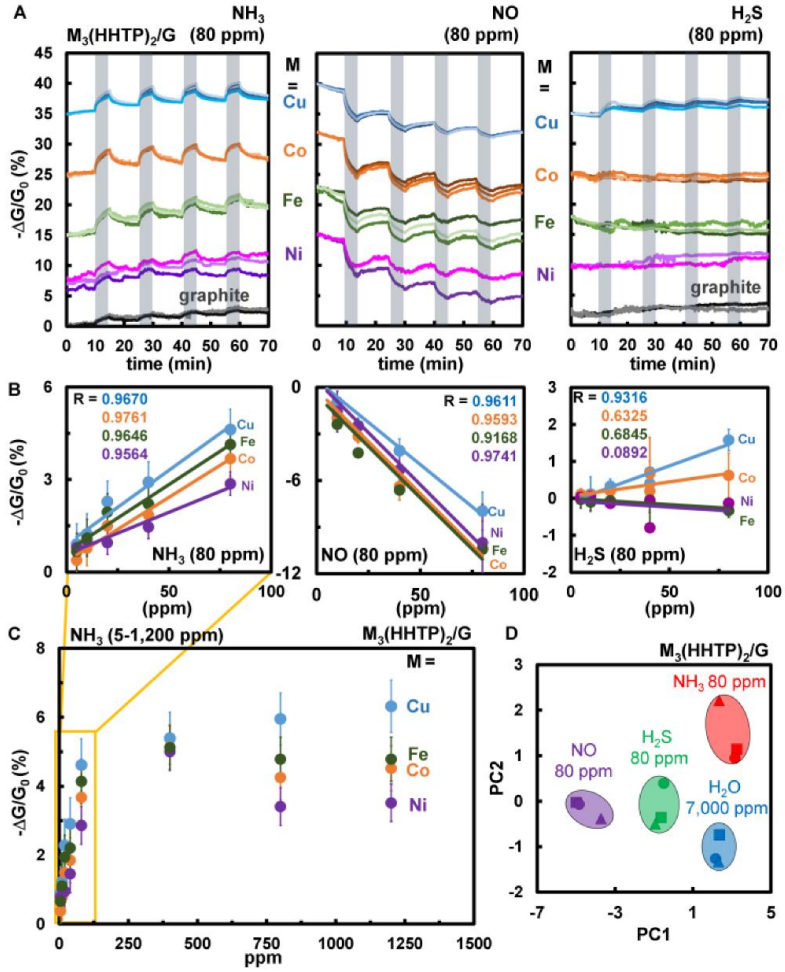

Figure 9. Sensing performances of M_3HHTP_2/graphite composites. ((**A**) Change in conductance ΔG/G0 (%) over time (min) for the M_3HHTP_2/graphite blends (Fe_3HHTP_2 = green, Co_3HHTP_2 = orange, Ni_3HHTP_2 = purple, Cu_3HHTP_2 = blue). (**B**) Concentration dependence plots of sensing response of the M_3HHTP_2/graphite blends to NH_3, NO and H_2S (5–80 ppm). (**C**) Sensing performance of M_3HHTP_2/graphite array towards different NH_3 concentrations (1200, 800, 80, 40, 20, 10, 5 ppm) diluted with N_2. (**D**) Ability of the array to distinguish between 80 ppm NH_3, H_2S, NO, and 7000 ppm H_2). Reproduced from Ref. [181].

4.6.4. Composites of MOFs with Conducting Polymers

Conducting polymers have been largely used as a material for preparing gas sensors [257], but they have usually exhibited poor sensitivity and selectivity. These drawbacks can be, to some extent, tackled by interfacing the polymers with MOFs. The polymerization of MOF with polymers is a possible procedure for modulating/modifying the properties of the parent polymer, while the addition of a polymer can improve the MOF water stability and strengthen the coordination bonds between the metal and the ligand [156].

To date, only few reports are focused on the gas-sensitive properties of MOF–polymer composites. For example, Sachdeva and coworkers prepared thin films of nano-NH_2-MIL-53(Al) dispersed in Matrimid 5218 for the development of VOC capacitive sensor devices [229]. They reported a detection limit of 1000 ppm for methanol, achieved thanks to the affinity of NH_2-MIL-53 (Al) for this specific alcohol. In addition, the prepared device exhibited cross-sensitivity and selectivity after exposition at 2×10^4 ppm to different VOCs (methanol, ethanol, and 2-propanol) and water.

Optical fibers with a ZIF-8/PDMS composite were employed by Cao et al. [240] for CH_4 detection in N_2. In the prepared system, polydimethylsiloxane (PDMS) polymer provides hydrophobicity, good mechanical properties and good permeability to CH_4, and the presence of ZIF-8 increased the free volume of the polymer and the CH_4 diffusion rate.

Other recent examples of polymer–MOF gas-sensitive composites include the preparation of MIL-101(Cr)PEDOT composites [219] employed for NO_2 sensing at a limit of detection as low as about 60 ppb, or the synthesis of a MOF−polymer mixed-matrix flexible membrane for H_2S detection at room temperature [209]. In the latter case, the sensing layer was produced embedding MOF-5 microparticles on a conductive chitosan (CS)-based membrane (the conductivity properties were inferred by a glycerol IL). The sensor showed a remarkable detection sensitivity for H_2S gas (as low as 1 ppm), fast response time (<8 s), recovery time of less than 30 s, and outstanding sensing stability, averaging at 97% detection with 50 ppm of H_2S gas.

Furthermore, Zhou et al. [237] synthesized a ZnO@ZIF-71(Co)@PDMS composite by allowing PDMS to polymerize on the surface of ZnO@ZIF-71. The material was used to develop a new chemiresistive sensor for VOCs, which showed high sensitivity, low detection limit, and high selectivity towards acetone and stability in the presence of humidity. The use of a PDMS coating allowed for the reduction in cross-sensitivity with ethanol.

5. Conclusions and Perspectives

The references reported in this review quite clearly demonstrate the ongoing interest in gas sensors employing ionic liquids and metal–organic frameworks. In the first case, the key actors are the sensing devices based on the amperometric principle (AGS), which started employing ILs as membrane-free electrolytes about 15 years ago. There are evident advantages offered by ILs, such as their high thermal stability, their wide electrochemical window and their low evaporation rate. Important challenges remain in order to maximize their technology-readiness level, up to the point where AGS systems/devices would be available at the commercial level. An obvious challenge is caused by the sensitivity of ILs to water, which "poisons" the electrolyte by affecting, in a relevant way, its viscosity. Hence, future developments have to confront a better understanding and management of the interaction of sensing devices with air and moisture. It is also worth mentioning that ILs are relatively expensive, so that another important trend for AGS devices is to miniaturize planar electrodes, i.e., obtaining cells with very small volumes (e.g., a few μL) in order to lower the cost of the electrolyte and, possibly, of the cells' manufacturing.

Despite the vast amount of scientific works regarding the use of MOFs for various applications, we realized while reviewing the literature on MOF-based gas sensors that several issues are still to be addressed, and that the literature available on the topic is still limited. Even if MOF-based sensors showed interesting and promising sensing properties, their sensing systems are rather complicated, and further enhancement in the transduction values of sensing signals is required. It is noteworthy that the available literature on

this topic is still too limited to catalyze and boost the development of modeling research aiming towards the description of the phenomena and the mechanisms involved in the sensing process.

Looking at the categories of MOF composites considered before for gas-sensing applications, we can draw some considerations:

- MOF materials employed for hybrid MOFs-MOXs composites are still limited; thus, the size of gas molecules that can be detected at present is also limited. Therefore, it is important to individuate other suitable MOF materials to be used instead of ZIF. Since the choice of MOX is dominated by ZnO due to the synthetic approach implemented, new methods of synthesis involving other MOXs as metal precursors have to be tested and other synthetic approaches have to be developed, also with the hope of improving more the sensing performance for specific gases.
- A surprisingly small number of reports is available on gas sensing based on MOF/carbon-based materials, if compared with the high number of studies in which this class of materials is employed as gas adsorbents. Such a limitation is probably partly related to the poor processability and to the synthetic approaches used, so research efforts in such a direction have to be prompted.
- Regarding MOF/polymer composites, there are few applications in gas sensing and the corresponding selection of MOF materials and polymers is also small. Such limitations are related to different aspects: MOFs have a certain pore size, and if the polymer is polymerized and inserted into the MOF pores, the transport of some gas molecules can be hampered and the accessibility of the target analyte to the active sites can be limited; the homogeneous dispersion of polymers in MOFs is, in most cases, far from being achieved and it still needs to be explored and optimized. In addition, the polymer-loading amount plays an important role in defining the final composite properties so various synthetic methods need to be further improved.

The integration of MOFs with conductive materials enables the detection of gas at room temperature in air, but the corresponding composites still exhibit poor sensing properties and cross-sensitivity, the range of detectable species is still limited to small molecules, and the response rate of the gas is slow due to diffusion phenomena. Moreover, little literature is still available on the development of sensors based on MOF composites for the detection of O_2 and industrial gases and for food security and health monitoring, since the research activities have, up to now, mostly focused on VOC detection. A further enhancement in the selectivity towards molecules with a similar sensing activity and the reduction in moisture sensitivity are only two of the main challenges to be pursued. Many of these challenges will likely require interdisciplinary research approaches to progress further. Overall, there is still more room for the development of such a kind of composite and it is our opinion that this is a direction worth exploring.

Author Contributions: Conceptualization, S.L.; methodology, S.L., M.A. and V.G.; data curation, V.G.; writing—original draft preparation, V.G., M.A., L.G. and S.L; writing—review and editing, all authors; project administration, S.L. All authors have read and agreed to the published version of the manuscript.

Funding: This research received no external funding.

Institutional Review Board Statement: Not applicable.

Informed Consent Statement: Not applicable.

Data Availability Statement: The data is available on the request from corresponding author.

Acknowledgments: M.A. and V.G. acknowledge the networking support by the COST Action CA19118 EsSENce, supported by the COST Association (European Cooperation in Science and Technology).

Conflicts of Interest: The authors declare no conflict of interest.

References

1. Gas and Particle Sensors–Technology and Market Trends 2021. Available online: https://www.i-micronews.com/products/gas-and-particle-sensors-technology-and-market-trends-2021/ (accessed on 9 April 2022).
2. Fortune Business Insights Industrial Gas Sensors Market Size, Growth | Industry Report 2026. Available online: https://www.fortunebusinessinsights.com/industry-reports/industrial-gas-sensors-market-101064 (accessed on 9 April 2022).
3. Barsan, N.; Koziej, D.; Weimar, U. Metal Oxide-Based Gas Sensor Research: How to? *Sens. Actuators B Chem.* **2007**, *121*, 18–35. [CrossRef]
4. Barsan, N.; Weimar, U. Conduction Model of Metal Oxide Gas Sensors. *J. Electroceram.* **2001**, *7*, 143–167. [CrossRef]
5. Korotcenkov, G. The Role of Morphology and Crystallographic Structure of Metal Oxides in Response of Conductometric-Type Gas Sensors. *Mater. Sci. Eng. R Rep.* **2008**, *61*, 1–39. [CrossRef]
6. Baron, R.; Saffell, J. Amperometric Gas Sensors as a Low Cost Emerging Technology Platform for Air Quality Monitoring Applications: A Review. *ACS Sens.* **2017**, *2*, 1553–1566. [CrossRef] [PubMed]
7. Lin, R.; Liu, S.; Ye, J.; Li, X.; Zhang, J. Photoluminescent Metal–Organic Frameworks for Gas Sensing. *Adv. Sci.* **2016**, *3*, 1500434. [CrossRef]
8. Wagner, T.; Haffer, S.; Weinberger, C.; Klaus, D.; Tiemann, M. Mesoporous Materials as Gas Sensors. *Chem. Soc. Rev.* **2013**, *42*, 4036–4053. [CrossRef]
9. Stetter, J.R.; Li, J. Amperometric Gas SensorsA Review. *Chem. Rev.* **2008**, *108*, 352–366. [CrossRef] [PubMed]
10. Malik, R.; Tomer, V.K.; Mishra, Y.K.; Lin, L. Functional Gas Sensing Nanomaterials: A Panoramic View. *Appl. Phys. Rev.* **2020**, *7*, 021301. [CrossRef]
11. Ghosh, R.; Gardner, J.W.; Guha, P.K. Air Pollution Monitoring Using Near Room Temperature Resistive Gas Sensors: A Review. *IEEE Trans. Electron. Devices* **2019**, *66*, 3254–3264. [CrossRef]
12. Halfaya, Y.; Bishop, C.; Soltani, A.; Sundaram, S.; Aubry, V.; Voss, P.L.; Salvestrini, J.-P.; Ougazzaden, A. Investigation of the Performance of HEMT-Based NO, NO_2 and NH_3 Exhaust Gas Sensors for Automotive Antipollution Systems. *Sensors* **2016**, *16*, 273. [CrossRef]
13. Wales, D.J.; Grand, J.; Ting, V.P.; Burke, R.D.; Edler, K.J.; Bowen, C.R.; Mintova, S.; Burrows, A.D. Gas Sensing Using Porous Materials for Automotive Applications. *Chem. Soc. Rev.* **2015**, *44*, 4290–4321. [CrossRef] [PubMed]
14. Kang, X.; Yip, S.; Meng, Y.; Wang, W.; Li, D.; Liu, C.; Ho, J.C. High-Performance Electrically Transduced Hazardous Gas Sensors Based on Low-Dimensional Nanomaterials. *Nanoscale Adv.* **2021**, *3*, 6254–6270. [CrossRef]
15. Horsfall, L.A.; Pugh, D.C.; Blackman, C.S.; Parkin, I.P. An Array of WO3 and CTO Heterojunction Semiconducting Metal Oxide Gas Sensors Used as a Tool for Explosive Detection. *J. Mater. Chem. A* **2017**, *5*, 2172–2179. [CrossRef]
16. Mirzaei, A.; Leonardi, S.G.; Neri, G. Detection of Hazardous Volatile Organic Compounds (VOCs) by Metal Oxide Nanostructures-Based Gas Sensors: A Review. *Ceram. Int.* **2016**, *42*, 15119–15141. [CrossRef]
17. Leidinger, M.; Sauerwald, T.; Reimringer, W.; Ventura, G.; Schütze, A. Selective Detection of Hazardous VOCs for Indoor Air Quality Applications Using a Virtual Gas Sensor Array. *J. Sens. Sens. Syst.* **2014**, *3*, 253–263. [CrossRef]
18. Chaisiwamongkhol, K.; Batchelor-McAuley, C.; Compton, R.G. Optimising Amperometric PH Sensing in Blood Samples: An Iridium Oxide Electrode for Blood PH Sensing. *Analyst* **2019**, *144*, 1386–1393. [CrossRef]
19. Landini, N.; Anania, G.; Fabbri, B.; Gaiardo, A.; Gherardi, S.; Guidi, V.; Rispoli, G.; Scagliarini, L.; Zonta, G.; Malagù, C. Neoplasms and Metastasis Detection in Human Blood Exhalations with a Device Composed by Nanostructured Sensors. *Sens. Actuators B Chem.* **2018**, *271*, 203–214. [CrossRef]
20. Galstyan, V.; Bhandari, M.P.; Sberveglieri, V.; Sberveglieri, G.; Comini, E. Metal Oxide Nanostructures in Food Applications: Quality Control and Packaging. *Chemosensors* **2018**, *6*, 16. [CrossRef]
21. Pallotti, D.; Orabona, E.; Amoruso, S.; Maddalena, P.; Lettieri, S. Modulation of Mixed-Phase Titania Photoluminescence by Oxygen Adsorption. *Appl. Phys. Lett.* **2014**, *105*, 031903. [CrossRef]
22. Gaiardo, A.; Fabbri, B.; Guidi, V.; Bellutti, P.; Giberti, A.; Gherardi, S.; Vanzetti, L.; Malagù, C.; Zonta, G. Metal Sulfides as Sensing Materials for Chemoresistive Gas Sensors. *Sensors* **2016**, *16*, 296. [CrossRef]
23. Ambrosone, G.; Coscia, U.; Lettieri, S.; Maddalena, P.; Privato, C.; Ferrero, S. Hydrogenated Amorphous Silicon Carbon Alloys for Solar Cells. *Thin Solid Film.* **2002**, *403*, 349–353. [CrossRef]
24. Comini, E. Metal Oxide Nano-Crystals for Gas Sensing. *Anal. Chim. Acta* **2006**, *568*, 28–40. [CrossRef] [PubMed]
25. Setaro, A.; Bismuto, A.; Lettieri, S.; Maddalena, P.; Comini, E.; Bianchi, S.; Baratto, C.; Sberveglieri, G. Optical Sensing of NO2 in Tin Oxide Nanowires at Sub-Ppm Level. *Sens. Actuators B Chem.* **2008**, *130*, 391–395. [CrossRef]
26. Setaro, A.; Lettieri, S.; Diamare, D.; Maddalena, P.; Malagù, C.; Carotta, M.C.; Martinelli, G. Nanograined Anatase Titania-Based Optochemical Gas Detection. *New J. Phys.* **2008**, *10*, 053030. [CrossRef]
27. Bittig, H.C.; Körtzinger, A.; Neill, C.; van Ooijen, E.; Plant, J.N.; Hahn, J.; Johnson, K.S.; Yang, B.; Emerson, S.R. Oxygen Optode Sensors: Principle, Characterization, Calibration, and Application in the Ocean. *Front. Mar. Sci.* **2018**, *4*, 429. [CrossRef]
28. Wang, X.; Wolfbeis, O.S. Optical Methods for Sensing and Imaging Oxygen: Materials, Spectroscopies and Applications. *Chem. Soc. Rev.* **2014**, *43*, 3666–3761. [CrossRef]
29. Quaranta, M.; Borisov, S.M.; Klimant, I. Indicators for Optical Oxygen Sensors. *Bioanal. Rev.* **2012**, *4*, 115–157. [CrossRef]
30. Clark, L.C.; Wolf, R.; Granger, D.; Taylor, Z. Continuous Recording of Blood Oxygen Tensions by Polarography. *J. Appl. Physiol.* **1953**, *6*, 189–193. [CrossRef]

31. Clark, J.L.C. Electrochemical Device for Chemical Analysis. U.S. Patent No. 2,913,386; Washington, DC: U.S. Patent and Trademark Office, 17 November 1959.
32. Xiong, L.; Compton, R.G. Amperometric Gas Detection: A Review. *Int. J. Electrochem. Sci.* **2014**, *9*, 30.
33. Vogel, W.M.; Lundquist, J.T. Reduction of Oxygen on Teflon-Bonded Platinum Electrodes. *J. Electrochem. Soc.* **1970**, *117*, 1512. [CrossRef]
34. Buzzeo, M.C.; Hardacre, C.; Compton, R.G. Use of Room Temperature Ionic Liquids in Gas Sensor Design. *Anal. Chem.* **2004**, *76*, 4583–4588. [CrossRef] [PubMed]
35. Gębicki, J.; Kloskowski, A.; Chrzanowski, W.; Stepnowski, P.; Namiesnik, J. Application of Ionic Liquids in Amperometric Gas Sensors. *Crit. Rev. Anal. Chem.* **2016**, *46*, 122–138. [CrossRef] [PubMed]
36. Gardecka, A.J.; Bishop, C.; Lee, D.; Corby, S.; Parkin, I.P.; Kafizas, A.; Krumdieck, S. High Efficiency Water Splitting Photoanodes Composed of Nano-Structured Anatase-Rutile TiO_2 Heterojunctions by Pulsed-Pressure MOCVD. *Appl. Catal. B Environ.* **2018**, *224*, 904–911. [CrossRef]
37. Preiß, E.M.; Rogge, T.; Krauß, A.; Seidel, H. Tin Oxide-Based Thin Films Prepared by Pulsed Laser Deposition for Gas Sensing. *Sens. Actuators B Chem.* **2016**, *236*, 865–873. [CrossRef]
38. Sanz, M.; Castillejo, M.; Amoruso, S.; Ausanio, G.; Bruzzese, R.; Wang, X. Ultra-Fast Laser Ablation and Deposition of TiO_2. *Appl. Phys. A* **2010**, *101*, 639–644. [CrossRef]
39. Sanz, M.; López-Arias, M.; Marco, J.F.; de Nalda, R.; Amoruso, S.; Ausanio, G.; Lettieri, S.; Bruzzese, R.; Wang, X.; Castillejo, M. Ultrafast Laser Ablation and Deposition of Wide Band Gap Semiconductors. *J. Phys. Chem. C* **2011**, *115*, 3203–3211. [CrossRef]
40. Coscia, U.; Ambrosone, G.; Lettieri, S.; Maddalena, P.; Rigato, V.; Restello, S.; Bobeico, E.; Tucci, M. Preparation of Microcrystalline Silicon–Carbon Films. *Sol. Energy Mater. Sol. Cells* **2005**, *87*, 433–444. [CrossRef]
41. Ambrosone, G.; Coscia, U.; Lettieri, S.; Maddalena, P.; Minarini, C. Optical, Structural and Electrical Properties of Mc-Si:H Films Deposited by SiH_4+H_2. *Mater. Sci. Eng. B* **2003**, *101*, 236–241. [CrossRef]
42. Parashar, M.; Shukla, V.K.; Singh, R. Metal Oxides Nanoparticles via Sol–Gel Method: A Review on Synthesis, Characterization and Applications. *J. Mater. Sci. Mater. Electron.* **2020**, *31*, 3729–3749. [CrossRef]
43. Esposito, S. "Traditional" Sol-Gel Chemistry as a Powerful Tool for the Preparation of Supported Metal and Metal Oxide Catalysts. *Materials* **2019**, *12*, 668. [CrossRef]
44. Liu, N.; Chen, X.; Zhang, J.; Schwank, J.W. A Review on TiO_2-Based Nanotubes Synthesized via Hydrothermal Method: Formation Mechanism, Structure Modification, and Photocatalytic Applications. *Catal. Today* **2014**, *225*, 34–51. [CrossRef]
45. Meyyappan, M. Carbon Nanotube-Based Chemical Sensors. *Small* **2016**, *12*, 2118–2129. [CrossRef] [PubMed]
46. Wang, T.; Huang, D.; Yang, Z.; Xu, S.; He, G.; Li, X.; Hu, N.; Yin, G.; He, D.; Zhang, L. A Review on Graphene-Based Gas/Vapor Sensors with Unique Properties and Potential Applications. *Nano. Micro. Lett.* **2016**, *8*, 95–119. [CrossRef]
47. Yang, S.; Jiang, C.; Wei, S. Gas Sensing in 2D Materials. *Appl. Phys. Rev.* **2017**, *4*, 021304. [CrossRef]
48. Koo, W.-T.; Jang, J.-S.; Kim, I.-D. Metal-Organic Frameworks for Chemiresistive Sensors. *Chem* **2019**, *5*, 1938–1963. [CrossRef]
49. Yao, M.-S.; Lv, X.-J.; Fu, Z.-H.; Li, W.-H.; Deng, W.-H.; Wu, G.-D.; Xu, G. Layer-by-Layer Assembled Conductive Metal–Organic Framework Nanofilms for Room-Temperature Chemiresistive Sensing. *Angew. Chem. Int. Ed.* **2017**, *56*, 16510–16514. [CrossRef] [PubMed]
50. Ando, M. Recent Advances in Optochemical Sensors for the Detection of H_2, O_2, O_3, CO, CO_2 and H_2O in Air. *TrAC Trends Anal. Chem.* **2006**, *25*, 937–948. [CrossRef]
51. Lettieri, S.; Pallotti, D.K.; Gesuele, F.; Maddalena, P. Unconventional Ratiometric-Enhanced Optical Sensing of Oxygen by Mixed-Phase TiO_2. *Appl. Phys. Lett.* **2016**, *109*, 031905. [CrossRef]
52. Popa, D.; Udrea, F. Towards Integrated Mid-Infrared Gas Sensors. *Sensors* **2019**, *19*, 2076. [CrossRef]
53. Nugroho, F.A.A.; Darmadi, I.; Cusinato, L.; Susarrey-Arce, A.; Schreuders, H.; Bannenberg, L.J.; da Silva Fanta, A.B.; Kadkhodazadeh, S.; Wagner, J.B.; Antosiewicz, T.J.; et al. Metal–Polymer Hybrid Nanomaterials for Plasmonic Ultrafast Hydrogen Detection. *Nat. Mater.* **2019**, *18*, 489–495. [CrossRef]
54. Lakowicz, J.R. (Ed.) Mechanisms and Dynamics of Fluorescence Quenching. In *Principles of Fluorescence Spectroscopy*; Springer: Boston, MA, USA, 2006; pp. 331–351. ISBN 978-0-387-46312-4.
55. Borbone, F.; Carella, A.; Caruso, U.; Roviello, G.; Tuzi, A.; Dardano, P.; Lettieri, S.; Maddalena, P.; Barsella, A. Large Second-Order NLO Activity in Poly(4-Vinylpyridine) Grafted with PdII and CuII Chromophoric Complexes with Tridentate Bent Ligands Containing Heterocycles. *Eur. J. Inorg. Chem.* **2008**, *2008*, 1846–1853. [CrossRef]
56. Bellani, S.; Ghadirzadeh, A.; Meda, L.; Savoini, A.; Tacca, A.; Marra, G.; Meira, R.; Morgado, J.; Di Fonzo, F.; Antognazza, M.R. Hybrid Organic/Inorganic Nanostructures for Highly Sensitive Photoelectrochemical Detection of Dissolved Oxygen in Aqueous Media. *Adv. Funct. Mater.* **2015**, *25*, 4531–4538. [CrossRef]
57. Li, C.; Ding, S.; Yang, L.; Zhu, Q.; Chen, M.; Tsang, D.C.W.; Cai, G.; Feng, C.; Wang, Y.; Zhang, C. Planar Optode: A Two-Dimensional Imaging Technique for Studying Spatial-Temporal Dynamics of Solutes in Sediment and Soil. *Earth Sci. Rev.* **2019**, *197*, 102916. [CrossRef]
58. Han, C.; Ren, J.; Tang, H.; Xu, D.; Xie, X. Quantitative Imaging of Radial Oxygen Loss from Valisneria Spiralis Roots with a Fluorescent Planar Optode. *Sci. Total Environ.* **2016**, *569*, 1232–1240. [CrossRef] [PubMed]
59. Jiang, Z.; Yu, X.; Hao, Y. Design and Fabrication of a Ratiometric Planar Optode for Simultaneous Imaging of PH and Oxygen. *Sensors* **2017**, *17*, 1316. [CrossRef]

60. Larsen, M.; Borisov, S.M.; Grunwald, B.; Klimant, I.; Glud, R.N. A Simple and Inexpensive High Resolution Color Ratiometric Planar Optode Imaging Approach: Application to Oxygen and PH Sensing.: A Simple RGB Based Planar Optode Imaging Approach. *Limnol. Oceanogr. Methods* **2011**, *9*, 348–360. [CrossRef]
61. Koren, K.; Moßhammer, M.; Scholz, V.V.; Borisov, S.M.; Holst, G.; Kühl, M. Luminescence Lifetime Imaging of Chemical Sensors—A Comparison between Time-Domain and Frequency-Domain Based Camera Systems. *Anal. Chem.* **2019**, *91*, 3233–3238. [CrossRef]
62. Christel, W.; Zhu, K.; Hoefer, C.; Kreuzeder, A.; Santner, J.; Bruun, S.; Magid, J.; Jensen, L.S. Spatiotemporal Dynamics of Phosphorus Release, Oxygen Consumption and Greenhouse Gas Emissions after Localised Soil Amendment with Organic Fertilisers. *Sci. Total Environ.* **2016**, *554*, 119–129. [CrossRef]
63. Pischedda, L.; Cuny, P.; Esteves, J.L.; Poggiale, J.-C.; Gilbert, F. Spatial Oxygen Heterogeneity in a Hediste Diversicolor Irrigated Burrow. *Hydrobiologia* **2012**, *1*, 109–124. [CrossRef]
64. Jiang, Z.; Yu, X.; Zhai, S.; Hao, Y. Ratiometric Dissolved Oxygen Sensors Based on Ruthenium Complex Doped with Silver Nanoparticles. *Sensors* **2017**, *17*, 548. [CrossRef]
65. Chu, C.-S. Optical Oxygen Sensing Properties of Ru(II) Complex and Porous Silica Nanoparticles Embedded in Solgel Matrix. *Appl. Opt. AO* **2011**, *50*, E145–E151. [CrossRef]
66. Cretì, A.; Valerini, D.; Taurino, A.; Quaranta, F.; Lomascolo, M.; Rella, R. Photoluminescence Quenching Processes by NO_2 Adsorption in ZnO Nanostructured Films. *J. Appl. Phys.* **2012**, *111*, 073520. [CrossRef]
67. Sanchez-Valencia, J.R.; Alcaire, M.; Romero-Gómez, P.; Macias-Montero, M.; Aparicio, F.J.; Borras, A.; Gonzalez-Elipe, A.R.; Barranco, A. Oxygen Optical Sensing in Gas and Liquids with Nanostructured ZnO Thin Films Based on Exciton Emission Detection. *J. Phys. Chem. C* **2014**, *118*, 9852–9859. [CrossRef]
68. Morandi, S.; Fioravanti, A.; Cerrato, G.; Lettieri, S.; Sacerdoti, M.; Carotta, M.C. Facile Synthesis of ZnO Nano-Structures: Morphology Influence on Electronic Properties. *Sens. Actuators B Chem.* **2017**, *249*, 581–589. [CrossRef]
69. Pallotti, D.K.; Passoni, L.; Gesuele, F.; Maddalena, P.; Di Fonzo, F.; Lettieri, S. Giant O_2—Induced Photoluminescence Modulation in Hierarchical Titanium Dioxide Nanostructures. *ACS Sens.* **2017**, *2*, 61–68. [CrossRef] [PubMed]
70. Siedl, N.; Koller, D.; Sternig, A.K.; Thomele, D.; Diwald, O. Photoluminescence Quenching in Compressed MgO Nanoparticle Systems. *Phys. Chem. Chem. Phys.* **2014**, *16*, 8339. [CrossRef]
71. Faglia, G.; Baratto, C.; Sberveglieri, G.; Zha, M.; Zappettini, A. Adsorption Effects of NO_2 at Ppm Level on Visible Photoluminescence Response of SnO_2 Nanobelts. *Appl. Phys. Lett.* **2005**, *86*, 011923. [CrossRef]
72. Trani, F.; Causà, M.; Lettieri, S.; Setaro, A.; Ninno, D.; Barone, V.; Maddalena, P. Role of Surface Oxygen Vacancies in Photoluminescence of Tin Dioxide Nanobelts. *Microelectron. J.* **2009**, *40*, 236–238. [CrossRef]
73. Lettieri, S.; Causà, M.; Setaro, A.; Trani, F.; Barone, V.; Ninno, D.; Maddalena, P. Direct Role of Surface Oxygen Vacancies in Visible Light Emission of Tin Dioxide Nanowires. *J. Chem. Phys.* **2008**, *129*, 244710. [CrossRef]
74. Lettieri, S.; Setaro, A.; Baratto, C.; Comini, E.; Faglia, G.; Sberveglieri, G.; Maddalena, P. On the Mechanism of Photoluminescence Quenching in Tin Dioxide Nanowires by NO_2 Adsorption. *New J. Phys.* **2008**, *10*, 043013. [CrossRef]
75. Lettieri, S.; Gargiulo, V.; Alfè, M.; Amati, M.; Zeller, P.; Maraloiu, V.-A.; Borbone, F.; Pavone, M.; Muñoz-García, A.B.; Maddalena, P. Simple Ethanol Refluxing Method for Production of Blue-Colored Titanium Dioxide with Oxygen Vacancies and Visible Light-Driven Photocatalytic Properties. *J. Phys. Chem. C* **2020**, *124*, 3564–3576. [CrossRef]
76. Lettieri, S.; Gargiulo, V.; Pallotti, D.K.; Vitiello, G.; Maddalena, P.; Alfè, M.; Marotta, R. Evidencing Opposite Charge-Transfer Processes at TiO_2 /Graphene-Related Materials Interface through a Combined EPR, Photoluminescence and Photocatalysis Assessment. *Catal. Today* **2018**, *315*, 19–30. [CrossRef]
77. Zhuang, W.; Hachem, K.; Bokov, D.; Javed Ansari, M.; Taghvaie Nakhjiri, A. Ionic Liquids in Pharmaceutical Industry: A Systematic Review on Applications and Future Perspectives. *J. Mol. Liq.* **2022**, *349*, 118145. [CrossRef]
78. Tanner, E.E.L. Ionic Liquids Charge Ahead. *Nat. Chem.* **2022**, *14*, 842. [CrossRef] [PubMed]
79. Buettner, C.S.; Cognigni, A.; Schröder, C.; Bica-Schröder, K. Surface-Active Ionic Liquids: A Review. *J. Mol. Liq.* **2022**, *347*, 118160. [CrossRef]
80. Plechkova, N.V.; Seddon, K.R. Applications of Ionic Liquids in the Chemical Industry. *Chem. Soc. Rev.* **2008**, *37*, 123–150. [CrossRef]
81. Schreiner, C.; Zugmann, S.; Hartl, R.; Gores, H.J. Fractional Walden Rule for Ionic Liquids: Examples from Recent Measurements and a Critique of the So-Called Ideal KCl Line for the Walden Plot. *J. Chem. Eng. Data* **2010**, *55*, 1784–1788. [CrossRef]
82. Ignat'ev, N.V.; Welz-Biermann, U.; Kucheryna, A.; Bissky, G.; Willner, H. New Ionic Liquids with Tris(Perfluoroalkyl)Trifluorophosphate (FAP) Anions. *J. Fluor. Chem.* **2005**, *126*, 1150–1159. [CrossRef]
83. Tang, Y.; Zeng, X. Electrochemical Oxidation of Hydrogen in Bis(Trifluoromethylsulfonyl)Imide Ionic Liquids under Anaerobic and Aerobic Conditions. *J. Phys. Chem. C* **2016**, *120*, 23542–23551. [CrossRef]
84. Lee, J.; Arrigan, D.W.M.; Silvester, D.S. Achievement of Prolonged Oxygen Detection in Room-Temperature Ionic Liquids on Mechanically Polished Platinum Screen-Printed Electrodes. *Anal. Chem.* **2016**, *88*, 5104–5111. [CrossRef]
85. Hussain, G.; O'Mullane, A.P.; Silvester, D.S. Modification of Microelectrode Arrays with High Surface Area Dendritic Platinum 3D Structures: Enhanced Sensitivity for Oxygen Detection in Ionic Liquids. *Nanomaterials* **2018**, *8*, 735. [CrossRef] [PubMed]
86. Lee, J.; Silvester, D.S. Low-Cost Microarray Thin-Film Electrodes with Ionic Liquid Gel-Polymer Electrolytes for Miniaturised Oxygen Sensing. *Analyst* **2016**, *141*, 3705–3713. [CrossRef] [PubMed]

87. Gondosiswanto, R.; Gunawan, C.A.; Hibbert, D.B.; Harper, J.B.; Zhao, C. Microcontact Printing of Thiol-Functionalized Ionic Liquid Microarrays for "Membrane-Less" and "Spill-Less" Gas Sensors. *ACS Appl. Mater. Interfaces* **2016**, *8*, 31368–31374. [CrossRef]
88. Liu, X.; Chen, X.; Xu, Y.; Chen, T.; Zeng, X. Effects of Water on Ionic Liquid Electrochemical Microsensor for Oxygen Sensing. *Sens. Actuators B Chem.* **2019**, *285*, 350–357. [CrossRef]
89. Wan, H.; Yin, H.; Mason, A.J. Rapid Measurement of Room Temperature Ionic Liquid Electrochemical Gas Sensor Using Transient Double Potential Amperometry. *Sens. Actuators B Chem.* **2017**, *242*, 658–666. [CrossRef] [PubMed]
90. Lee, J.; Hussain, G.; Banks, C.E.; Silvester, D.S. Screen-Printed Graphite Electrodes as Low-Cost Devices for Oxygen Gas Detection in Room-Temperature Ionic Liquids. *Sensors* **2017**, *17*, 2734. [CrossRef]
91. Gondosiswanto, R.; Hibbert, D.B.; Fang, Y.; Zhao, C. Ionic Liquid Microstrips Impregnated with Magnetic Nanostirrers for Sensitive Gas Sensors. *ACS Appl. Mater. Interfaces* **2017**, *9*, 43377–43385. [CrossRef]
92. Lin, L.; Zeng, X. Toward Continuous Amperometric Gas Sensing in Ionic Liquids: Rationalization of Signal Drift Nature and Calibration Methods. *Anal. Bioanal. Chem.* **2018**, *410*, 4587–4596. [CrossRef]
93. Gondosiswanto, R.; Hibbert, D.B.; Fang, Y.; Zhao, C. Redox Recycling Amplification Using an Interdigitated Microelectrode Array for Ionic Liquid-Based Oxygen Sensors. *Anal. Chem.* **2018**, *90*, 3950–3957. [CrossRef]
94. Liu, Y.; Liu, J.; Liu, Q.; Zhang, H.; Li, Z.; Jing, X.; Yuan, Y.; Zhang, H.; Liu, P.; Wang, J. Ionic Liquids Combined with Pt-Modified Ordered Mesoporous Carbons as Electrolytes for the Oxygen Sensing. *Sens. Actuators B Chem.* **2018**, *254*, 490–501. [CrossRef]
95. Zhang, H.; Liu, J.; Liu, Q.; Chen, R.; Zhang, H.; Yu, J.; Song, D.; Jing, X.; Zhang, M.; Wang, J. Electrochemical Oxygen Sensor Based on the Interaction of Double-Layer Ionic Liquid Film (DLILF). *J. Electrochem. Soc.* **2018**, *165*, B779. [CrossRef]
96. Yu, L.; Liu, J.; Yin, W.; Yu, J.; Chen, R.; Song, D.; Liu, Q.; Li, R.; Wang, J. Ionic Liquid Combined with $NiCo_2O_4$/RGO Enhances Electrochemical Oxygen Sensing. *Talanta* **2020**, *209*, 120515. [CrossRef] [PubMed]
97. Yin, W.; Liu, J.; Liu, Q.; Chen, R.; Yu, J.; Zhang, H.; Song, D.; Fan, M.; Zhang, M.; Wang, J. Ag-CS Enhanced Performance of Pyrrolidone-Based Ionic Liquid Oxygen Sensor. *J. Electrochem. Soc.* **2020**, *167*, 067522. [CrossRef]
98. Wan, H.; Liu, X.; Wang, X.; Chen, Y.; Wang, P.P. Facile Screen-Printed Carbon Nanotube Electrode on Porous Substrate with Gold Nanoparticle Modification for Rapid Electrochemical Gas Sensing. *J. Electrochem. Soc.* **2021**, *168*, 067514. [CrossRef]
99. Yin, W.; Alali, K.T.; Zhang, M.; Liu, J.; Song, D.; Liu, Q.; Yu, J.; Chen, R.; Zhang, H.; Wang, J. A−Fe_2O_3/RGO Cooperated with Tri-Alkyl-Substituted-Imidazolium Ionic Liquids for Enhancing Oxygen Sensing. *Sens. Actuators B Chem.* **2021**, *341*, 130029. [CrossRef]
100. Doblinger, S.; Hay, C.E.; Tomé, L.C.; Mecerreyes, D.; Silvester, D.S. Ionic Liquid/Poly(Ionic Liquid) Membranes as Non-Flowing, Conductive Materials for Electrochemical Gas Sensing. *Anal. Chim. Acta* **2022**, *1195*, 339414. [CrossRef]
101. Lee, J.; Hussain, G.; López-Salas, N.; MacFarlane, D.R.; Silvester, D.S. Thin Films of Poly(Vinylidene Fluoride-*Co*-Hexafluoropropylene)-Ionic Liquid Mixtures as Amperometric Gas Sensing Materials for Oxygen and Ammonia. *Analyst* **2020**, *145*, 1915–1924. [CrossRef]
102. Liu, X.; Chen, X.; Ju, J.; Wang, X.; Mei, Z.; Qu, H.; Xu, Y.; Zeng, X. Platinum–Nickel Bimetallic Nanosphere–Ionic Liquid Interface for Electrochemical Oxygen and Hydrogen Sensing. *ACS Appl. Nano Mater.* **2019**, *2*, 2958–2968. [CrossRef]
103. Tang, Y.; He, J.; Gao, X.; Yang, T.; Zeng, X. Continuous Amperometric Hydrogen Gas Sensing in Ionic Liquids. *Analyst* **2018**, *143*, 4136–4146. [CrossRef]
104. Jayanthi, E.; Murugesan, N.; Suneesh, A.S.; Ramesh, C.; Anthonysamy, S. Sensing Behavior of Room Temperature Amperometric H_2 Sensor with Pd Electrodeposited from Ionic Liquid Electrolyte as Sensing Electrode. *J. Electrochem. Soc.* **2017**, *164*, H5210. [CrossRef]
105. Zhi, Z.; Gao, W.; Yang, J.; Geng, C.; Yang, B.; Tian, C.; Fan, S.; Li, H.; Li, J.; Hua, Z. Amperometric Hydrogen Gas Sensor Based on Pt/C/Nafion Electrode and Ionic Electrolyte. *Sens. Actuators B Chem.* **2022**, *367*, 132137. [CrossRef]
106. Hussain, G.; Ge, M.; Zhao, C.; Silvester, D.S. Fast Responding Hydrogen Gas Sensors Using Platinum Nanoparticle Modified Microchannels and Ionic Liquids. *Anal. Chim. Acta* **2019**, *1072*, 35–45. [CrossRef]
107. Hussain, G.; Silvester, D.S. Comparison of Voltammetric Techniques for Ammonia Sensing in Ionic Liquids. *Electroanalysis* **2018**, *30*, 75–83. [CrossRef]
108. Hussain, G.; Silvester, D.S. Detection of Sub-Ppm Concentrations of Ammonia in an Ionic Liquid: Enhanced Current Density Using "Filled" Recessed Microarrays. *Anal. Chem.* **2016**, *88*, 12453–12460. [CrossRef] [PubMed]
109. Hussain, G.; Aldous, L.; Silvester, D.S. Preparation of Platinum-Based 'cauliflower Microarrays' for Enhanced Ammonia Gas Sensing. *Anal. Chim. Acta* **2019**, *1048*, 12–21. [CrossRef] [PubMed]
110. Ge, M.; Hussain, G.; Hibbert, D.B.; Silvester, D.S.; Zhao, C. Ionic Liquid-Based Microchannels for Highly Sensitive and Fast Amperometric Detection of Toxic Gases. *Electroanalysis* **2019**, *31*, 66–74. [CrossRef]
111. Chi, X.; Tang, Y.; Zeng, X. Electrode Reactions Coupled with Chemical Reactions of Oxygen, Water and Acetaldehyde in an Ionic Liquid: New Approaches for Sensing Volatile Organic Compounds. *Electrochim. Acta* **2016**, *216*, 171–180. [CrossRef]
112. Ge, M.; Gondosiswanto, R.; Zhao, C. Electrodeposited Copper Nanoparticles in Ionic Liquid Microchannels Electrode for Carbon Dioxide Sensor. *Inorg. Chem. Commun.* **2019**, *107*, 107458. [CrossRef]
113. Toniolo, R.; Dossi, N.; Bortolomeazzi, R.; Bonazza, G.; Daniele, S. Volatile Aldehydes Sensing in Headspace Using a Room Temperature Ionic Liquid-Modified Electrochemical Microprobe. *Talanta* **2019**, *197*, 522–529. [CrossRef]

114. Gil-González, N.; Benito-Lopez, F.; Castaño, E.; Morant-Miñana, M.C. Imidazole-Based Ionogel as Room Temperature Benzene and Formaldehyde Sensor. *Microchim. Acta* **2020**, *187*, 638. [CrossRef]
115. Doblinger, S.; Lee, J.; Gurnah, Z.; Silvester, D.S. Detection of Sulfur Dioxide at Low Parts-per-Million Concentrations Using Low-Cost Planar Electrodes with Ionic Liquid Electrolytes. *Anal. Chim. Acta* **2020**, *1124*, 156–165. [CrossRef] [PubMed]
116. Esteves, C.; Palma, S.I.C.J.; Costa, H.M.A.; Alves, C.; Santos, G.M.C.; Ramou, E.; Carvalho, A.L.; Alves, V.; Roque, A.C.A. Tackling Humidity with Designer Ionic Liquid-Based Gas Sensing Soft Materials. *Adv. Mater.* **2022**, *34*, 2107205. [CrossRef]
117. Zuliani, I.; Fattori, A.; Svigelj, R.; Dossi, N.; Grazioli, C.; Bontempelli, G.; Toniolo, R. Amperometric Detection of Ethanol Vapors by Screen Printed Electrodes Modified by Paper Crowns Soaked with Room Temperature Ionic Liquids. *Electroanalysis* **2022**, *34*, 1–11. [CrossRef]
118. Gao, J.; Hua, Z.; Xu, S.; Wan, H.; Zhi, Z.; Chen, X.; Fan, S. Amperometric Gas Sensors Based on Screen Printed Electrodes with Porous Ceramic Substrates. *Sens. Actuators B Chem.* **2021**, *342*, 130045. [CrossRef]
119. Luo, R.; Wu, Y.; Li, Q.; Du, B.; Zhou, S.; Li, H. Rational Synthesis and Characterization of IL-CNTs-PANI Microporous Polymer Electrolyte Film. *Synth. Met.* **2021**, *274*, 116720. [CrossRef]
120. Kuberský, P.; Navrátil, J.; Syrový, T.; Sedlák, P.; Nešpůrek, S.; Hamáček, A. An Electrochemical Amperometric Ethylene Sensor with Solid Polymer Electrolyte Based on Ionic Liquid. *Sensors* **2021**, *21*, 711. [CrossRef]
121. Zhang, S.-Y.; Zhuang, Q.; Zhang, M.; Wang, H.; Gao, Z.; Sun, J.-K.; Yuan, J. Poly(Ionic Liquid) Composites. *Chem. Soc. Rev.* **2020**, *49*, 1726–1755. [CrossRef]
122. Silvester, D.S. New Innovations in Ionic Liquid–Based Miniaturised Amperometric Gas Sensors. *Curr. Opin. Electrochem.* **2019**, *15*, 7–17. [CrossRef]
123. Raptopoulou, C.P. Metal-Organic Frameworks: Synthetic Methods and Potential Applications. *Materials* **2021**, *14*, 310. [CrossRef]
124. Andirova, D.; Cogswell, C.F.; Lei, Y.; Choi, S. Effect of the Structural Constituents of Metal Organic Frameworks on Carbon Dioxide Capture. *Microporous Mesoporous Mater.* **2016**, *219*, 276–305. [CrossRef]
125. Yulia, F.; Nasruddin; Zulys, A.; Ruliandini, R. Metal-Organic Framework Based Chromium Terephthalate (MIL-101 Cr) Growth for Carbon Dioxide Capture: A Review. *J. Adv. Res. Fluid Mech. Therm. Sci.* **2019**, *57*, 158–174.
126. Ding, M.; Cai, X.; Jiang, H.-L. Improving MOF Stability: Approaches and Applications. *Chem. Sci.* **2019**, *10*, 10209–10230. [CrossRef] [PubMed]
127. Jiao, L.; Seow, J.Y.R.; Skinner, W.S.; Wang, Z.U.; Jiang, H.-L. Metal–Organic Frameworks: Structures and Functional Applications. *Mater. Today* **2019**, *27*, 43–68. [CrossRef]
128. Lee, Y.-R.; Kim, J.; Ahn, W.-S. Synthesis of Metal-Organic Frameworks: A Mini Review. *Korean J. Chem. Eng.* **2013**, *30*, 1667–1680. [CrossRef]
129. Silva, P.; Vilela, S.M.F.; Tomé, J.P.C.; Almeida Paz, F.A. Multifunctional Metal–Organic Frameworks: From Academia to Industrial Applications. *Chem. Soc. Rev.* **2015**, *44*, 6774–6803. [CrossRef]
130. Safaei, M.; Foroughi, M.M.; Ebrahimpoor, N.; Jahani, S.; Omidi, A.; Khatami, M. A Review on Metal-Organic Frameworks: Synthesis and Applications. *TrAC Trends Anal. Chem.* **2019**, *118*, 401–425. [CrossRef]
131. Freund, R.; Zaremba, O.; Arnauts, G.; Ameloot, R.; Skorupskii, G.; Dincă, M.; Bavykina, A.; Gascon, J.; Ejsmont, A.; Goscianska, J.; et al. The Current Status of MOF and COF Applications. *Angew. Chem. Int. Ed.* **2021**, *60*, 23975–24001. [CrossRef]
132. Song, Y.; Li, X.; Sun, L.; Wang, L. Metal/Metal Oxide Nanostructures Derived from Metal–Organic Frameworks. *RSC Adv.* **2015**, *5*, 7267–7279. [CrossRef]
133. Alfè, M.; Gargiulo, V.; Amati, M.; Maraloiu, V.-A.; Maddalena, P.; Lettieri, S. Mesoporous TiO_2 from Metal-Organic Frameworks for Photoluminescence-Based Optical Sensing of Oxygen. *Catalysts* **2021**, *11*, 795. [CrossRef]
134. Tan, X.; Wu, Y.; Lin, X.; Zeb, A.; Xu, X.; Luo, Y.; Liu, J. Application of MOF-Derived Transition Metal Oxides and Composites as Anodes for Lithium-Ion Batteries. *Inorg. Chem. Front.* **2020**, *7*, 4939–4955. [CrossRef]
135. Li, H.-Y.; Zhao, S.-N.; Zang, S.-Q.; Li, J. Functional Metal–Organic Frameworks as Effective Sensors of Gases and Volatile Compounds. *Chem. Soc. Rev.* **2020**, *49*, 6364–6401. [CrossRef] [PubMed]
136. Li, Y.; Xiao, A.-S.; Zou, B.; Zhang, H.-X.; Yan, K.-L.; Lin, Y. Advances of Metal–Organic Frameworks for Gas Sensing. *Polyhedron* **2018**, *154*, 83–97. [CrossRef]
137. Huang, B.; Li, Y.; Zeng, W. Application of Metal-Organic Framework-Based Composites for Gas Sensing and Effects of Synthesis Strategies on Gas-Sensitive Performance. *Chemosensors* **2021**, *9*, 226. [CrossRef]
138. Sosa, J.; Bennett, T.; Nelms, K.; Liu, B.; Tovar, R.; Liu, Y. Metal–Organic Framework Hybrid Materials and Their Applications. *Crystals* **2018**, *8*, 325. [CrossRef]
139. Mandal, S.; Natarajan, S.; Mani, P.; Pankajakshan, A. Post-Synthetic Modification of Metal–Organic Frameworks Toward Applications. *Adv. Funct. Mater.* **2021**, *31*, 2006291. [CrossRef]
140. Alfe, M.; Policicchio, A.; Lisi, L.; Gargiulo, V. Solid Sorbents for CO_2 and CH_4 Adsorption: The Effect of Metal Organic Framework Hybridization with Graphene-like Layers on the Gas Sorption Capacities at High Pressure. *Renew. Sustain. Energy Rev.* **2021**, *141*, 110816. [CrossRef]
141. Lei, J.; Qian, R.; Ling, P.; Cui, L.; Ju, H. Design and Sensing Applications of Metal–Organic Framework Composites. *TrAC Trends Anal. Chem.* **2014**, *58*, 71–78. [CrossRef]
142. Zhu, Q.-L.; Xu, Q. Metal–Organic Framework Composites. *Chem. Soc. Rev.* **2014**, *43*, 5468–5512. [CrossRef]

143. Kalaj, M.; Bentz, K.C.; Ayala, S.; Palomba, J.M.; Barcus, K.S.; Katayama, Y.; Cohen, S.M. MOF-Polymer Hybrid Materials: From Simple Composites to Tailored Architectures. *Chem. Rev.* **2020**, *120*, 8267–8302. [CrossRef]
144. Wang, X.; Wang, Y.; Ying, Y. Recent Advances in Sensing Applications of Metal Nanoparticle/Metal–Organic Framework Composites. *TrAC Trends Anal. Chem.* **2021**, *143*, 116395. [CrossRef]
145. Chen, C.; Li, B.; Zhou, L.; Xia, Z.; Feng, N.; Ding, J.; Wang, L.; Wan, H.; Guan, G. Synthesis of Hierarchically Structured Hybrid Materials by Controlled Self-Assembly of Metal–Organic Framework with Mesoporous Silica for CO_2 Adsorption. *ACS Appl. Mater. Interfaces* **2017**, *9*, 23060–23071. [CrossRef] [PubMed]
146. Chronopoulos, D.D.; Saini, H.; Tantis, I.; Zbořil, R.; Jayaramulu, K.; Otyepka, M. Carbon Nanotube Based Metal–Organic Framework Hybrids From Fundamentals Toward Applications. *Small* **2022**, *18*, 2104628. [CrossRef]
147. Zheng, Y.; Zheng, S.; Xue, H.; Pang, H. Metal-Organic Frameworks/Graphene-Based Materials: Preparations and Applications. *Adv. Funct. Mater.* **2018**, *28*, 1804950. [CrossRef]
148. Alfè, M.; Gargiulo, V.; Lisi, L.; Di Capua, R. Synthesis and Characterization of Conductive Copper-Based Metal-Organic Framework/Graphene-like Composites. *Mater. Chem. Phys.* **2014**, *147*, 744–750. [CrossRef]
149. Aguilera-Sigalat, J.; Bradshaw, D. Synthesis and Applications of Metal-Organic Framework–Quantum Dot (QD@MOF) Composites. *Coord. Chem. Rev.* **2016**, *307*, 267–291. [CrossRef]
150. Li, S.; Huo, F. Metal–Organic Framework Composites: From Fundamentals to Applications. *Nanoscale* **2015**, *7*, 7482–7501. [CrossRef] [PubMed]
151. Jahan, M.; Bao, Q.; Yang, J.-X.; Loh, K.P. Structure-Directing Role of Graphene in the Synthesis of Metal–Organic Framework Nanowire. *J. Am. Chem. Soc.* **2010**, *132*, 14487–14495. [CrossRef]
152. Li, X.; Zhang, Z.; Xiao, W.; Deng, S.; Chen, C.; Zhang, N. Mechanochemistry-Assisted Encapsulation of Metal Nanoparticles in MOF Matrices via a Sacrificial Strategy. *J. Mater. Chem. A* **2019**, *7*, 14504–14509. [CrossRef]
153. Chen, L.; Chen, H.; Luque, R.; Li, Y. Metal−organic Framework Encapsulated Pd Nanoparticles: Towards Advanced Heterogeneous Catalysts. *Chem. Sci.* **2014**, *5*, 3708–3714. [CrossRef]
154. Hu, M.-L.; Razavi, S.A.A.; Piroozzadeh, M.; Morsali, A. Sensing Organic Analytes by Metal–Organic Frameworks: A New Way of Considering the Topic. *Inorg. Chem. Front.* **2020**, *7*, 1598–1632. [CrossRef]
155. Small, L.J.; Schindelholz, M.E.; Nenoff, T.M. Hold on Tight: MOF-Based Irreversible Gas Sensors. *Ind. Eng. Chem. Res.* **2021**, *60*, 7998–8006. [CrossRef]
156. Zhang, R.; Lu, L.; Chang, Y.; Liu, M. Gas Sensing Based on Metal-Organic Frameworks: Concepts, Functions, and Developments. *J. Hazard. Mater.* **2022**, *429*, 128321. [CrossRef] [PubMed]
157. Kumar, P.; Deep, A.; Kim, K.-H. Metal Organic Frameworks for Sensing Applications. *TrAC Trends Anal. Chem.* **2015**, *73*, 39–53. [CrossRef]
158. Bhardwaj, S.K.; Bhardwaj, N.; Kaur, R.; Mehta, J.; Sharma, A.L.; Kim, K.-H.; Deep, A. An Overview of Different Strategies to Introduce Conductivity in Metal–Organic Frameworks and Miscellaneous Applications Thereof. *J. Mater. Chem. A* **2018**, *6*, 14992–15009. [CrossRef]
159. Razavi, S.A.A.; Masoomi, M.Y.; Morsali, A. Stimuli-Responsive Metal-Organic Framework (MOF) with Chemo-Switchable Properties for Colorimetric Detection of $CHCl_3$. *Chem. Eur. J.* **2017**, *23*, 12559–12564. [CrossRef]
160. Wang, H.; Lustig, W.P.; Li, J. Sensing and Capture of Toxic and Hazardous Gases and Vapors by Metal–Organic Frameworks. *Chem. Soc. Rev.* **2018**, *47*, 4729–4756. [CrossRef]
161. Diamantis, S.A.; Margariti, A.; Pournara, A.D.; Papaefstathiou, G.S.; Manos, M.J.; Lazarides, T. Luminescent Metal–Organic Frameworks as Chemical Sensors: Common Pitfalls and Proposed Best Practices. *Inorg. Chem. Front.* **2018**, *5*, 1493–1511. [CrossRef]
162. Mahata, P.; Mondal, S.K.; Singha, D.K.; Majee, P. Luminescent Rare-Earth-Based MOFs as Optical Sensors. *Dalton Trans.* **2017**, *46*, 301–328. [CrossRef]
163. Huangfu, M.; Wang, M.; Lin, C.; Wang, J.; Wu, P. Luminescent Metal–Organic Frameworks as Chemical Sensors Based on "Mechanism–Response": A Review. *Dalton Trans.* **2021**, *50*, 3429–3449. [CrossRef]
164. Chen, L.; Liu, D.; Peng, J.; Du, Q.; He, H. Ratiometric Fluorescence Sensing of Metal-Organic Frameworks: Tactics and Perspectives. *Coord. Chem. Rev.* **2020**, *404*, 213113. [CrossRef]
165. Zhang, Y.; Yuan, S.; Day, G.; Wang, X.; Yang, X.; Zhou, H.-C. Luminescent Sensors Based on Metal-Organic Frameworks. *Coord. Chem. Rev.* **2018**, *354*, 28–45. [CrossRef]
166. Zhu, C.; Gerald, R.E.; Huang, J. Metal-Organic Framework Materials Coupled to Optical Fibers for Chemical Sensing: A Review. *IEEE Sens. J.* **2021**, *21*, 19647–19661. [CrossRef] [PubMed]
167. Kim, K.-J.; Lu, P.; Culp, J.T.; Ohodnicki, P.R. Metal–Organic Framework Thin Film Coated Optical Fiber Sensors: A Novel Waveguide-Based Chemical Sensing Platform. *ACS Sens.* **2018**, *3*, 386–394. [CrossRef] [PubMed]
168. Kreno, L.E.; Hupp, J.T.; Van Duyne, R.P. Metal−Organic Framework Thin Film for Enhanced Localized Surface Plasmon Resonance Gas Sensing. *Anal. Chem.* **2010**, *82*, 8042–8046. [CrossRef]
169. He, C.; Liu, L.; Korposh, S.; Correia, R.; Morgan, S.P. Volatile Organic Compound Vapour Measurements Using a Localised Surface Plasmon Resonance Optical Fibre Sensor Decorated with a Metal-Organic Framework. *Sensors* **2021**, *21*, 1420. [CrossRef]
170. Na Songkhla, S.; Nakamoto, T. Overview of Quartz Crystal Microbalance Behavior Analysis and Measurement. *Chemosensors* **2021**, *9*, 350. [CrossRef]

171. Wang, L. Metal-Organic Frameworks for QCM-Based Gas Sensors: A Review. *Sens. Actuators A Phys.* **2020**, *307*, 111984. [CrossRef]
172. Ma, Z.; Yuan, T.; Fan, Y.; Wang, L.; Duan, Z.; Du, W.; Zhang, D.; Xu, J. A Benzene Vapor Sensor Based on a Metal-Organic Framework-Modified Quartz Crystal Microbalance. *Sens. Actuators B Chem.* **2020**, *311*, 127365. [CrossRef]
173. Mandal, D.; Banerjee, S. Surface Acoustic Wave (SAW) Sensors: Physics, Materials, and Applications. *Sensors* **2022**, *22*, 820. [CrossRef]
174. Paschke, B.; Wixforth, A.; Denysenko, D.; Volkmer, D. Fast Surface Acoustic Wave-Based Sensors to Investigate the Kinetics of Gas Uptake in Ultra-Microporous Frameworks. *ACS Sens.* **2017**, *2*, 740–747. [CrossRef]
175. Devkota, J.; Greve, D.W.; Hong, T.; Kim, K.-J.; Ohodnicki, P.R. An 860 MHz Wireless Surface Acoustic Wave Sensor with a Metal-Organic Framework Sensing Layer for CO_2 and CH_4. *IEEE Sens. J.* **2020**, *20*, 9740–9747. [CrossRef]
176. Vanotti, M.; Poisson, S.; Blondeau-Patissier, V.; André, L.; Brandès, S.; Desbois, N.; Gros, C.P. SAW Based CO_2 Sensor: Influence of Functionalizing MOF Crystal Size on the Sensor's Selectivity. In Proceedings of the International Conference on Advances in Sensors, Actuators, Metering and Sensing, Nice, France, 18–22 July 2021.
177. Vashist, D.S.K.; Tewari, R.; Bajpai, D.R.P.; Bharadwaj, D.L.M.; Raiteri, R. A Review of Microcantilevers for Sensing Applications. *J. Nanotechnol.* **2007**, *3*, 15. [CrossRef]
178. Cai, S.; Li, W.; Xu, P.; Xia, X.; Yu, H.; Zhang, S.; Li, X. In Situ Construction of Metal–Organic Framework (MOF) UiO-66 Film on Parylene-Patterned Resonant Microcantilever for Trace Organophosphorus Molecules Detection. *Analyst* **2019**, *144*, 3729–3735. [CrossRef] [PubMed]
179. Yim, C.; Lee, M.; Yun, M.; Kim, G.-H.; Kim, K.T.; Jeon, S. CO_2-Selective Nanoporous Metal-Organic Framework Microcantilevers. *Sci. Rep.* **2015**, *5*, 10674. [CrossRef]
180. Ellern, I.; Venkatasubramanian, A.; Lee, J.H.; Hesketh, P.J.; Stavilla, V.; Allendorf, M.D.; Robinson, A.L. Characterization of Piezoresistive Microcantilever Sensors with Metal Organic Frameworks for the Detection of Volatile Organic Compounds. *ECS Trans.* **2013**, *50*, 469–476. [CrossRef]
181. Ko, M.; Aykanat, A.; Smith, M.; Mirica, K. Drawing Sensors with Ball-Milled Blends of Metal-Organic Frameworks and Graphite. *Sensors* **2017**, *17*, 2192. [CrossRef]
182. Chen, E.-X.; Yang, H.; Zhang, J. Zeolitic Imidazolate Framework as Formaldehyde Gas Sensor. *Inorg. Chem.* **2014**, *53*, 5411–5413. [CrossRef]
183. Chidambaram, A.; Stylianou, K.C. Electronic Metal–Organic Framework Sensors. *Inorg. Chem. Front.* **2018**, *5*, 979–998. [CrossRef]
184. Liu, J.; Sun, F.; Zhang, F.; Wang, Z.; Zhang, R.; Wang, C.; Qiu, S. In Situ Growth of Continuous Thin Metal–Organic Framework Film for Capacitive Humidity Sensing. *J. Mater. Chem.* **2011**, *21*, 3775. [CrossRef]
185. Sapsanis, C.; Omran, H.; Chernikova, V.; Shekhah, O.; Belmabkhout, Y.; Buttner, U.; Eddaoudi, M.; Salama, K. Insights on Capacitive Interdigitated Electrodes Coated with MOF Thin Films: Humidity and VOCs Sensing as a Case Study. *Sensors* **2015**, *15*, 18153–18166. [CrossRef]
186. Assen, A.H.; Yassine, O.; Shekhah, O.; Eddaoudi, M.; Salama, K.N. MOFs for the Sensitive Detection of Ammonia: Deployment of Fcu-MOF Thin Films as Effective Chemical Capacitive Sensors. *ACS Sens.* **2017**, *2*, 1294–1301. [CrossRef] [PubMed]
187. Yassine, O.; Shekhah, O.; Assen, A.H.; Belmabkhout, Y.; Salama, K.N.; Eddaoudi, M. H_2S Sensors: Fumarate-Based Fcu-MOF Thin Film Grown on a Capacitive Interdigitated Electrode. *Angew. Chem. Int. Ed.* **2016**, *55*, 15879–15883. [CrossRef] [PubMed]
188. Homayoonnia, S.; Zeinali, S. Design and Fabrication of Capacitive Nanosensor Based on MOF Nanoparticles as Sensing Layer for VOCs Detection. *Sens. Actuators B Chem.* **2016**, *237*, 776–786. [CrossRef]
189. Achmann, S.; Hagen, G.; Kita, J.; Malkowsky, I.; Kiener, C.; Moos, R. Metal-Organic Frameworks for Sensing Applications in the Gas Phase. *Sensors* **2009**, *9*, 1574–1589. [CrossRef]
190. Weiss, A.; Reimer, N.; Stock, N.; Tiemann, M.; Wagner, T. Screening of Mixed-Linker CAU-10 MOF Materials for Humidity Sensing by Impedance Spectroscopy. *Microporous Mesoporous Mater.* **2016**, *220*, 39–43. [CrossRef]
191. Zhang, Y.; Chen, Y.; Zhang, Y.; Cong, H.; Fu, B.; Wen, S.; Ruan, S. A Novel Humidity Sensor Based on NH_2-MIL-125(Ti) Metal Organic Framework with High Responsiveness. *J. Nanopart. Res.* **2013**, *15*, 2014. [CrossRef]
192. D'Amico, A.; Di Natale, C.; Paolesse, R.; Mantini, A.; Goletti, C.; Davide, F.; Filosofi, G. Chemical Sensing Materials Characterization by Kelvin Probe Technique. *Sens. Actuators B Chem.* **2000**, *70*, 254–262. [CrossRef]
193. Davydovskaya, P.; Pentyala, V.; Yurchenko, O.; Hussein, L.; Pohle, R.; Urban, G.A. Work Function Based Sensing of Alkanes and Alcohols with Benzene Tricarboxylate Linked Metal Organic Frameworks. *Sens. Actuators B Chem.* **2014**, *193*, 911–917. [CrossRef]
194. Pentyala, V.; Davydovskaya, P.; Pohle, R.; Urban, G.; Yurchenko, O. Mg-MOF74 and Co-MOF74 as Sensing Layers for CO_2 Detection. *Procedia Eng.* **2014**, *87*, 1071–1074. [CrossRef]
195. Zhang, W.; Xiong, R.-G. Ferroelectric Metal–Organic Frameworks. *Chem. Rev.* **2012**, *112*, 1163–1195. [CrossRef]
196. Han, S.; Kim, H.; Kim, J.; Jung, Y. Modulating the Magnetic Behavior of Fe(II)–MOF-74 by the High Electron Affinity of the Guest Molecule. *Phys. Chem. Chem. Phys.* **2015**, *17*, 16977–16982. [CrossRef] [PubMed]
197. Chen, X.; Behboodian, R.; Bagnall, D.; Taheri, M.; Nasiri, N. Metal-Organic-Frameworks: Low Temperature Gas Sensing and Air Quality Monitoring. *Chemosensors* **2021**, *9*, 316. [CrossRef]
198. Huang, X.; Gong, Z.; Lv, Y. Advances in Metal-Organic Frameworks-Based Gas Sensors for Hazardous Substances. *TrAC Trends Anal. Chem.* **2022**, *153*, 116644. [CrossRef]
199. Majhi, S.M.; Ali, A.; Rai, P.; Greish, Y.E.; Alzamly, A.; Surya, S.G.; Qamhieh, N.; Mahmoud, S.T. Metal–Organic Frameworks for Advanced Transducer Based Gas Sensors: Review and Perspectives. *Nanoscale Adv.* **2022**, *4*, 697–732. [CrossRef]

200. Olorunyomi, J.F.; Geh, S.T.; Caruso, R.A.; Doherty, C.M. Metal–Organic Frameworks for Chemical Sensing Devices. *Mater. Horiz.* **2021**, *8*, 2387–2419. [CrossRef] [PubMed]
201. Drobek, M.; Kim, J.-H.; Bechelany, M.; Vallicari, C.; Julbe, A.; Kim, S.S. MOF-Based Membrane Encapsulated ZnO Nanowires for Enhanced Gas Sensor Selectivity. *ACS Appl. Mater. Interfaces* **2016**, *8*, 8323–8328. [CrossRef] [PubMed]
202. Wu, X.; Xiong, S.; Mao, Z.; Hu, S.; Long, X. A Designed ZnO@ZIF-8 Core-Shell Nanorod Film as a Gas Sensor with Excellent Selectivity for H $_2$ over CO. *Chem. Eur. J.* **2017**, *23*, 7969–7975. [CrossRef]
203. Cui, F.; Chen, W.; Jin, L.; Zhang, H.; Jiang, Z.; Song, Z. Fabrication of ZIF-8 Encapsulated ZnO Microrods with Enhanced Sensing Properties for H_2 Detection. *J. Mater. Sci. Mater. Electron.* **2018**, *29*, 19697–19709. [CrossRef]
204. Zhou, T.; Sang, Y.; Wang, X.; Wu, C.; Zeng, D.; Xie, C. Pore Size Dependent Gas-Sensing Selectivity Based on ZnO@ZIF Nanorod Arrays. *Sens. Actuators B Chem.* **2018**, *258*, 1099–1106. [CrossRef]
205. Koo, W.-T.; Qiao, S.; Ogata, A.F.; Jha, G.; Jang, J.-S.; Chen, V.T.; Kim, I.-D.; Penner, R.M. Accelerating Palladium Nanowire H_2 Sensors Using Engineered Nanofiltration. *ACS Nano* **2017**, *11*, 9276–9285. [CrossRef]
206. Weber, M.; Kim, J.-H.; Lee, J.-H.; Kim, J.-Y.; Iatsunskyi, I.; Coy, E.; Drobek, M.; Julbe, A.; Bechelany, M.; Kim, S.S. High-Performance Nanowire Hydrogen Sensors by Exploiting the Synergistic Effect of Pd Nanoparticles and Metal–Organic Framework Membranes. *ACS Appl. Mater. Interfaces* **2018**, *10*, 34765–34773. [CrossRef]
207. Kumar, A.; Mohammadi, M.M.; Zhao, Y.; Liu, Y.; Liu, J.; Thundat, T.; Swihart, M.T. Reduced Graphene Oxide-Wrapped Palladium Nanowires Coated with a Layer of Zeolitic Imidazolate Framework-8 for Hydrogen Sensing. *ACS Appl. Nano Mater.* **2021**, *4*, 8081–8093. [CrossRef]
208. Lv, R.; Zhang, Q.; Wang, W.; Lin, Y.; Zhang, S. ZnO@ZIF-8 Core-Shell Structure Gas Sensors with Excellent Selectivity to H_2. *Sensors* **2021**, *21*, 4069. [CrossRef] [PubMed]
209. Ali, A.; Alzamly, A.; Greish, Y.E.; Bakiro, M.; Nguyen, H.L.; Mahmoud, S.T. A Highly Sensitive and Flexible Metal–Organic Framework Polymer-Based H_2S Gas Sensor. *ACS Omega* **2021**, *6*, 17690–17697. [CrossRef] [PubMed]
210. Xie, B.; Ding, B.; Mao, P.; Wang, Y.; Liu, Y.; Chen, M.; Zhou, C.; Wen, H.; Xia, S.; Han, M.; et al. Metal Nanocluster—Metal Organic Framework—Polymer Hybrid Nanomaterials for Improved Hydrogen Detection. *Small* **2022**, *18*, 2200634. [CrossRef]
211. Hwang, S.I.; Sopher, E.M.; Zeng, Z.; Schulte, Z.M.; White, D.L.; Rosi, N.L.; Star, A. Metal–Organic Frameworks on Palladium Nanoparticle–Functionalized Carbon Nanotubes for Monitoring Hydrogen Storage. *ACS Appl. Nano Mater.* **2022**. [CrossRef]
212. DMello, M.E.; Sundaram, N.G.; Kalidindi, S.B. Assembly of ZIF-67 Metal-Organic Framework over Tin Oxide Nanoparticles for Synergistic Chemiresistive CO $_2$ Gas Sensing. *Chem. Eur. J.* **2018**, *24*, 9220–9223. [CrossRef]
213. Jayaramulu, K.; Esclance DMello, M.; Kesavan, K.; Schneemann, A.; Otyepka, M.; Kment, S.; Narayana, C.; Kalidindi, S.B.; Varma, R.S.; Zboril, R.; et al. A Multifunctional Covalently Linked Graphene–MOF Hybrid as an Effective Chemiresistive Gas Sensor. *J. Mater. Chem. A* **2021**, *9*, 17434–17441. [CrossRef]
214. Liu, Y.; Wang, R.; Zhang, T.; Liu, S.; Fei, T. Zeolitic Imidazolate Framework-8 (ZIF-8)-Coated In_2O_3 Nanofibers as an Efficient Sensing Material for Ppb-Level NO_2 Detection. *J. Colloid Interface Sci.* **2019**, *541*, 249–257. [CrossRef]
215. Jo, Y.-M.; Lim, K.; Yoon, J.W.; Jo, Y.K.; Moon, Y.K.; Jang, H.W.; Lee, J.-H. Visible-Light-Activated Type II Heterojunction in Cu_3 (Hexahydroxytriphenylene)$_2$/Fe_2O_3 Hybrids for Reversible NO_2 Sensing: Critical Role of π–Π* Transition. *ACS Cent. Sci.* **2021**, *7*, 1176–1182. [CrossRef]
216. Koo, W.; Kim, S.; Jang, J.; Kim, D.; Kim, I. Catalytic Metal Nanoparticles Embedded in Conductive Metal–Organic Frameworks for Chemiresistors: Highly Active and Conductive Porous Materials. *Adv. Sci.* **2019**, *6*, 1900250. [CrossRef] [PubMed]
217. Kim, J.-O.; Koo, W.-T.; Kim, H.; Park, C.; Lee, T.; Hutomo, C.A.; Choi, S.Q.; Kim, D.S.; Kim, I.-D.; Park, S. Large-Area Synthesis of Nanoscopic Catalyst-Decorated Conductive MOF Film Using Microfluidic-Based Solution Shearing. *Nat. Commun.* **2021**, *12*, 4294. [CrossRef] [PubMed]
218. He, L.; Zhang, W.; Wu, H.; Zhao, Y. Zn–Co Zeolitic Imidazolate Framework Nanoparticles Intercalated in Graphene Nanosheets for Room-Temperature NO_2 Sensing. *ACS Appl. Nano Mater.* **2021**, *4*, 3998–4006. [CrossRef]
219. Le Ouay, B.; Boudot, M.; Kitao, T.; Yanagida, T.; Kitagawa, S.; Uemura, T. Nanostructuration of PEDOT in Porous Coordination Polymers for Tunable Porosity and Conductivity. *J. Am. Chem. Soc.* **2016**, *138*, 10088–10091. [CrossRef] [PubMed]
220. Zhou, Y.; Zhou, T.; Zhang, Y.; Tang, L.; Guo, Q.; Wang, M.; Xie, C.; Zeng, D. Synthesis of Core-Shell Flower-like WO3@ZIF-71 with Enhanced Response and Selectivity to H_2S Gas. *Solid State Ion.* **2020**, *350*, 115278. [CrossRef]
221. Wu, X.; Xiong, S.; Gong, Y.; Gong, Y.; Wu, W.; Mao, Z.; Liu, Q.; Hu, S.; Long, X. MOF-SMO Hybrids as a H_2S Sensor with Superior Sensitivity and Selectivity. *Sens. Actuators B Chem.* **2019**, *292*, 32–39. [CrossRef]
222. Tan, J.; Hussain, S.; Ge, C.; Zhan, M.; Liu, J.; Liu, S.; Liu, G.; Qiao, G. Construction of Hierarchical Trimetallic Organic Framework Leaf-like Nanostructures Derived from Carbon Nanotubes for Gas-Sensing Applications. *J. Hazard. Mater.* **2020**, *400*, 123155. [CrossRef]
223. Travlou, N.A.; Singh, K.; Rodríguez-Castellón, E.; Bandosz, T.J. Cu–BTC MOF–Graphene-Based Hybrid Materials as Low Concentration Ammonia Sensors. *J. Mater. Chem. A* **2015**, *3*, 11417–11429. [CrossRef]
224. Yin, Y.; Zhang, H.; Huang, P.; Xiang, C.; Zou, Y.; Xu, F.; Sun, L. Inducement of Nanoscale Cu–BTC on Nanocomposite of PPy–RGO and Its Performance in Ammonia Sensing. *Mater. Res. Bull.* **2018**, *99*, 152–160. [CrossRef]
225. Khan, F.U.; Mehmood, S.; Zhao, X.; Yang, Y.; Pan, X. Ultra-Sensitive Bimetallic Alloy Loaded with Porous Architecture MOF for Ammonia Detection at Room Temperature. In Proceedings of the 2021 IEEE International Symposium on Circuits and Systems (ISCAS), Daegu, Korea, 22–28 May 2021; IEEE: Piscataway, NJ, USA; pp. 1–5.

226. Bhardwaj, S.K.; Mohanta, G.C.; Sharma, A.L.; Kim, K.-H.; Deep, A. A Three-Phase Copper MOF-Graphene-Polyaniline Composite for Effective Sensing of Ammonia. *Anal. Chim. Acta* **2018**, *1043*, 89–97. [CrossRef]
227. Garg, N.; Kumar, M.; Kumari, N.; Deep, A.; Sharma, A.L. Chemoresistive Room-Temperature Sensing of Ammonia Using Zeolite Imidazole Framework and Reduced Graphene Oxide (ZIF-67/RGO) Composite. *ACS Omega* **2020**, *5*, 27492–27501. [CrossRef] [PubMed]
228. Feng, S.; Jia, X.; Yang, J.; Li, Y.; Wang, S.; Song, H. One-Pot Synthesis of Core–Shell ZIF-8@ZnO Porous Nanospheres with Improved Ethanol Gas Sensing. *J. Mater. Sci. Mater. Electron.* **2020**, *31*, 22534–22545. [CrossRef]
229. Sachdeva, S.; Koper, S.J.H.; Sabetghadam, A.; Soccol, D.; Gravesteijn, D.J.; Kapteijn, F.; Sudhölter, E.J.R.; Gascon, J.; de Smet, L.C.P.M. Gas Phase Sensing of Alcohols by Metal Organic Framework–Polymer Composite Materials. *ACS Appl. Mater. Interfaces* **2017**, *9*, 24926–24935. [CrossRef] [PubMed]
230. Jafari, N.; Zeinali, S. Highly Rapid and Sensitive Formaldehyde Detection at Room Temperature Using a ZIF-8/MWCNT Nanocomposite. *ACS Omega* **2020**, *5*, 4395–4402. [CrossRef] [PubMed]
231. Jafari, N.; Zeinali, S.; Shadmehr, J. Room Temperature Resistive Gas Sensor Based on ZIF-8/MWCNT/AgNPs Nanocomposite for VOCs Detection. *J. Mater. Sci. Mater. Electron.* **2019**, *30*, 12339–12350. [CrossRef]
232. Tian, H.; Fan, H.; Li, M.; Ma, L. Zeolitic Imidazolate Framework Coated ZnO Nanorods as Molecular Sieving to Improve Selectivity of Formaldehyde Gas Sensor. *ACS Sens.* **2016**, *1*, 243–250. [CrossRef]
233. Jagan Mohan Reddy, A.; Katari, N.K.; Nagaraju, P.; Hussain Reddy, K.; Surendra Babu, M.S. Fabrication and Deployment of Nanodisc ZnO@ZIF-8, ZnO@NA and ZnO@INA Core–Shell MOFs: Enhanced NH_3 and HCHO Gas Sensing. *J. Mater. Sci. Mater. Electron.* **2021**, *32*, 7827–7840. [CrossRef]
234. Wang, D.; Li, Z.; Zhou, J.; Fang, H.; He, X.; Jena, P.; Zeng, J.-B.; Wang, W.-N. Simultaneous Detection and Removal of Formaldehyde at Room Temperature: Janus Au@ZnO@ZIF-8 Nanoparticles. *Nano-Micro Lett.* **2018**, *10*, 4. [CrossRef]
235. Yao, M.-S.; Tang, W.-X.; Wang, G.-E.; Nath, B.; Xu, G. MOF Thin Film-Coated Metal Oxide Nanowire Array: Significantly Improved Chemiresistor Sensor Performance. *Adv. Mater.* **2016**, *28*, 5229–5234. [CrossRef]
236. Zhou, T.; Sang, Y.; Sun, Y.; Wu, C.; Wang, X.; Tang, X.; Zhang, T.; Wang, H.; Xie, C.; Zeng, D. Gas Adsorption at Metal Sites for Enhancing Gas Sensing Performance of ZnO@ZIF-71 Nanorod Arrays. *Langmuir* **2019**, *35*, 3248–3255. [CrossRef]
237. Zhou, T.; Dong, W.; Qiu, Y.; Chen, S.; Wang, X.; Xie, C.; Zeng, D. Selectivity of a ZnO@ZIF-71@PDMS Nanorod Array Gas Sensor Enhanced by Coating a Polymer Selective Separation Membrane. *ACS Appl. Mater. Interfaces* **2021**, *13*, 54589–54596. [CrossRef] [PubMed]
238. Qin, Y.; Xie, J.; Liu, S.; Bai, Y. Selective Methanol-Sensing of SnS-Supported Ultrathin ZIF-8 Nanocomposite with Core-Shell Heterostructure. *Sens. Actuators B Chem.* **2022**, *368*, 132230. [CrossRef]
239. Nair, S.S.; Illyaskutty, N.; Tam, B.; Yazaydin, A.O.; Emmerich, K.; Steudel, A.; Hashem, T.; Schöttner, L.; Wöll, C.; Kohler, H.; et al. ZnO@ZIF-8: Gas Sensitive Core-Shell Hetero-Structures Show Reduced Cross-Sensitivity to Humidity. *Sens. Actuators B Chem.* **2020**, *304*, 127184. [CrossRef]
240. Cao, R.; Ding, H.; Kim, K.-J.; Peng, Z.; Wu, J.; Culp, J.T.; Ohodnicki, P.R.; Beckman, E.; Chen, K.P. Metal-Organic Framework Functionalized Polymer Coating for Fiber Optical Methane Sensors. *Sens. Actuators B Chem.* **2020**, *324*, 128627. [CrossRef]
241. Hong, T.; Culp, J.; Kim, K.-J.; Ohodnicki, P.R. Polymer/Metal–Organic Framework Composite Sensors for Gas Detection. *Meet. Abstr.* **2019**, *MA2019-01*, 2028. [CrossRef]
242. Zheng, L.; Keppler, N.; Zhang, H.; Behrens, P.; Roth, B. Planar Polymer Optical Waveguide with Metal-Organic Framework Coating for Carbon Dioxide Sensing. *Adv Mater. Technol.* **2022**, 2200395. [CrossRef]
243. Kong, Y.; Zhao, Z.; Wang, Y.; Yang, S.; Huang, G.; Wang, Y.; Liu, C.; You, C.; Tan, J.; Wang, C.; et al. Integration of a Metal–Organic Framework Film with a Tubular Whispering-Gallery-Mode Microcavity for Effective CO_2 Sensing. *ACS Appl. Mater. Interfaces* **2021**, *13*, 58104–58113. [CrossRef]
244. Chong, X.; Kim, K.; Zhang, Y.; Li, E.; Ohodnicki, P.R.; Chang, C.-H.; Wang, A.X. Plasmonic Nanopatch Array with Integrated Metal–Organic Framework for Enhanced Infrared Absorption Gas Sensing. *Nanotechnology* **2017**, *28*, 26LT01. [CrossRef]
245. Zhang, J.; Yue, D.; Xia, T.; Cui, Y.; Yang, Y.; Qian, G. A Luminescent Metal-Organic Framework Film Fabricated on Porous Al_2O_3 Substrate for Sensitive Detecting Ammonia. *Microporous Mesoporous Mater.* **2017**, *253*, 146–150. [CrossRef]
246. Wong, D.; Abuzalat, O.; Mostafa, S.; Park, S.S.; Kim, S. Intense Pulsed Light-Based Synthesis of Hybrid TiO_2–SnO_2 /MWCNT Doped Cu-BTC for Room Temperature Ammonia Sensing. *J. Mater. Chem. C* **2020**, *8*, 7567–7574. [CrossRef]
247. Chappanda, K.N.; Shekhah, O.; Yassine, O.; Patole, S.P.; Eddaoudi, M.; Salama, K.N. The Quest for Highly Sensitive QCM Humidity Sensors: The Coating of CNT/MOF Composite Sensing Films as Case Study. *Sens. Actuators B Chem.* **2018**, *257*, 609–619. [CrossRef]
248. Xu, X.-Y.; Yan, B. Eu(III)-Functionalized ZnO@MOF Heterostructures: Integration of Pre-Concentration and Efficient Charge Transfer for the Fabrication of a Ppb-Level Sensing Platform for Volatile Aldehyde Gases in Vehicles. *J. Mater. Chem. A* **2017**, *5*, 2215–2223. [CrossRef]
249. Zhai, L.; Yang, Z.-X.; Zhang, W.-W.; Zuo, J.-L.; Ren, X.-M. Dual-Emission and Thermochromic Luminescence Alkaline Earth Metal Coordination Polymers and Their Blend Films with Polyvinylidene Fluoride for Detecting Nitrobenzene Vapor. *J. Mater. Chem. C* **2018**, *6*, 7030–7041. [CrossRef]
250. Kouser, S.; Hezam, A.; Khadri, M.J.N.; Khanum, S.A. A Review on Zeolite Imidazole Frameworks: Synthesis, Properties, and Applications. *J. Porous Mater.* **2022**, *29*, 663–681. [CrossRef]

251. Yao, M.-S.; Cao, L.-A.; Tang, Y.-X.; Wang, G.-E.; Liu, R.-H.; Kumar, P.N.; Wu, G.-D.; Deng, W.-H.; Hong, W.-J.; Xu, G. Gas Transport Regulation in a MO/MOF Interface for Enhanced Selective Gas Detection. *J. Mater. Chem. A* **2019**, *7*, 18397–18403. [CrossRef]
252. Wang, A.; Wang, C.; Fu, L.; Wong-Ng, W.; Lan, Y. Recent Advances of Graphitic Carbon Nitride-Based Structures and Applications in Catalyst, Sensing, Imaging, and LEDs. *Nano Micro Lett.* **2017**, *9*, 47. [CrossRef]
253. Chen, Z.; Wang, J.; Wang, Y. Strategies for the Performance Enhancement of Graphene-Based Gas Sensors: A Review. *Talanta* **2021**, *235*, 122745. [CrossRef]
254. Han, T.; Nag, A.; Chandra Mukhopadhyay, S.; Xu, Y. Carbon Nanotubes and Its Gas-Sensing Applications: A Review. *Sens. Actuators A Phys.* **2019**, *291*, 107–143. [CrossRef]
255. Gargiulo, V.; Alfano, B.; Di Capua, R.; Alfé, M.; Vorokhta, M.; Polichetti, T.; Massera, E.; Miglietta, M.L.; Schiattarella, C.; Di Francia, G. Graphene-like Layers as Promising Chemiresistive Sensing Material for Detection of Alcohols at Low Concentration. *J. Appl. Phys.* **2018**, *123*, 024503. [CrossRef]
256. Villani, F.; Loffredo, F.; Alfano, B.; Miglietta, M.L.; Verdoliva, L.; Alfè, M.; Gargiulo, V.; Polichetti, T. Graphene-Like Based-Chemiresistors Inkjet-Printed onto Paper Substrate. In *Sensors*; Andò, B., Baldini, F., Di Natale, C., Ferrari, V., Marletta, V., Marrazza, G., Militello, V., Miolo, G., Rossi, M., Scalise, L., et al., Eds.; Lecture Notes in Electrical Engineering; Springer International Publishing: Cham, Germany, 2019; Volume 539, pp. 337–343. ISBN 978-3-030-04323-0.
257. Bai, H.; Shi, G. Gas Sensors Based on Conducting Polymers. *Sensors* **2007**, *7*, 267–307. [CrossRef]